NOVA SCHOOL OF SCIENCE & TECHNOLOGY

DEPARTAMENT OF MATERIALS SCIENCE

DAVID MIGUEL HENRIQUES BENTO

BSc in Micro and Nanotechnology Engineering

TOWARDS SOFT ROBOTICS: 3D PRINTED HYDROGELS WITH PHOTO-THERMAL ACTUATION

MASTER IN MICRO AND NANOTECHNOLOGY ENGINEERING

NOVA University Lisbon

September, 2022

DEPARTAMENT OF
MATERIALS SCIENCE

TOWARDS SOFT ROBOTICS: 3D PRINTED HYDROGELS WITH PHOTO-THERMAL ACTUATION

DAVID MIGUEL HENRIQUES BENTO

BSc in Micro and Nanotechnology Engineering

Adviser: Brigitte Maria Städler
Associate Professor, Aarhus University

Co-advisers: João Paulo Miranda Ribeiro Borges
Associate Professor with Habilitation, NOVA University Lisbon

Examination Committee:

Chair: Rui Alberto Garção Barreira do Nascimento Igreja,
Assistant Professor, FCT-NOVA

Rapporteurs: Pedro Lúcio Maia Marques de Almeida,
Adjunct Professor, ISEL

Adviser: João Paulo Miranda Ribeiro Borges,
Associate Professor with Habilitation, FCT-NOVA

MASTER IN MICRO AND NANOTECHNOLOGY ENGINEERING

NOVA University Lisbon
September, 2022

Towards soft robotics: 3D printed hydrogels with photo-thermal actuation.

Para os meus pais.

ACKNOWLEDGMENTS

My journey throughout university was filled with amazing people who inspired me to reach higher and helped me cultivate my love for science and research and become a better version of myself. I would like to acknowledge my thesis advisor Prof. Dr Brigitte Städler, for accepting me into her fantastic Laboratory for Cell Mimicry group and inviting me to work on such an exciting project. I would like to acknowledge my thesis co-advisor Prof. Dr João Borges, for always giving me help and support when I needed it and for always believing in me. I would like to acknowledge the Interdisciplinary Nanoscience Center (iNANO) and Aarhus University for accepting me as a master's thesis student and letting me study at such incredible facilities.

Special thanks to the Laboratory for Cell Mimicry, in particular to Stefan Pendlmayr, who accompanied me during the thesis, taught me about 3D printing, and sharpened my critical thinking. Special thanks to Miguel Ramos for all the SEM and TEM images and for all knowledge regarding metallic nanoparticles. Additionally, I would like to thank Stephan and Miguel for helping me review this thesis, without them, this would not be possible. Special thanks to Edit Brodszkij for teaching me all about PNIPAM and for helping me functionalize it. Special thanks to Jacob Nyemann from the Department of Physics and Astronomy at Aarhus University for helping me with the light source characterization. I would like to acknowledge NOVA School of Science and Technology, the Department of Material Science and all its great professors for giving me access to a stimulating environment where I could grow as an individual and meet some of my best friends. I would like to acknowledge Prof. Dr Rodrigo Martins and Prof. Dr Elvira Fortunato for creating the bachelor and master's in Micro and Nanotechnology Engineering.

Obrigado a todos os que me aturaram ao longo destes árduos cinco anos, especialmente aos que tiveram paciência quando eu não a tive. Obrigado aos meus pais por me sempre suportarem e sempre encorajarem a querer mais e não me contentar com pouco. Obrigado, João, por seres o melhor amigo que alguém poderia ter. Quem não nos conhecesse até podia dizer que eramos gémeos. Obrigado às minhas avó, tia e prima por me mostrarem que há coisas mais importantes na vida para além do trabalho. Obrigado, Claúdia, por teres puxado a melhor versão de mim e por me fazeres companhia quando me sentia sozinho, mesmo quando não estavas presente. Por me mostrares que acima de tudo o meu melhor amigo sou eu próprio e por estares sempre comigo até nos momentos mais difíceis. Obrigado, Maria, por teres sempre um ombro e um sofá disponível para mim. Por sempre alinhares nos planos extravagantes de última hora. Obrigado, Espetáculo, por sempre estarem lá para mim. Obrigado, Carlos, por me dares uma voz quando já não conseguia falar. Obrigado, André, por me sempre fazeres sentir incluído. Obrigado, Joana, por ouvires todas as minhas lamechices. Obrigado, Catita, por todas as vezes que me ligaste com dúvidas existenciais. Obrigado, Catarina, por… por tudo um pouco na verdade. Obrigado, Chiara, por mesmo estando tão longe conseguiste estar tão perto. E obrigado a todos os afilhados oficiais e não-oficiais e à finalmente à minha madrinha, que me convenceu a fazer a tese em Erasmus. Obrigado a todos os que me acompanharam neste percurso. Ultrapassando um perigo iminente de cada vez.

“Para ser grande, sê inteiro: nada
Teu exagera ou exclui.
Sê todo em cada coisa. Põe quanto és
No mínimo que fazes.
Assim em cada lago a lua toda
Brilha, porque alta vive.”
(Fernando Pessoa).

"Impossible means that you haven't found the solution yet."
(Henry Ford)

ABSTRACT

Conventional robotics are based on rigid materials, such as stiff plastics, composites, metals, and ceramics. This makes them resilient and efficient at handling high loads and repetitive tasks. However, these robots still struggle with autonomy, as most need to be connected to a power supply. This either makes them static or coupled to a heavy battery, which is not favorable for locomotion. Thus a new field of robotics emerged, one that took inspiration from nature. To achieve this, the hard matter was substituted for soft matter, and by mimicking simple living organisms, i.e. plants and gastropods, the new soft robots could move, grasp and sense. Nevertheless, there are still challenges to overcome. Actuation is still very limited and slow, which makes moving inefficient. This work aims to study possible ways to create soft robots able to move vertically, either by swimming or jumping, by light actuation. To achieve the movement PNIPAM-based hydrogels were embedded with gold nanostars to function as photo-thermal converters. PNIPAM is known for its rapid thermal response, which results in the rapid expulsion of water for temperatures above its lowest critical solubility temperature. Together with 3D printing, this property can be exploited to create hydrogels capable of bending and relaxing. If done in quick succession, it could translate into vertical movement. 3D printed structures resulted in soft actuators capable of going from a flat initial state to a 400° curvature, with a thermal stimulus of 44 °C. With light stimulation, the gold nanostar-embedded hydrogels were able to raise their temperature 3.6 °C per min. In an aqueous environment, a 2 °C rise and a curvature of 26° were obtained after 2 min of light stimulation. It is possible to conclude that the heat generated by the gold nanostars is not sufficient to actuate the soft robots in an aqueous environment due to the heat dissipating into the water.

Keywords: Soft robotics, hydrogels, PNIPAM, gold nanostars, 3D printed, light-responsive.

RESUMO

A robótica convencional está fundamentada em materiais rígidos, como plásticos, compósitos, metais e cerâmicas. O que resulta em robôs resilientes e eficazes para manuseio de cargas pesadas e a realização de tarefas repetitivas. Contudo, estes robôs têm a desvantagem de falta autonomia, pois a maioria precisa de estar conectada a uma fonte de alimentação, o que os torna estáticos, ou acoplados a uma bateria pesada, não favorecendo a sua locomoção. Assim, criou-se um campo na robótica inspirado pela natureza, substituindo a matéria dura por matéria mole. Imitando organismos simples, como plantas e gastrópodes, os novos *soft robots* foram capazes de se deslocar, agarrar e sentir. Apesar disso, ainda há desafios a serem superados. A atuação ainda é muito limitada e lenta, o que torna a movimentação ineficiente. Este trabalho visa estudar possíveis formas de tornar *soft robots* capazes de se mover verticalmente, seja nadando ou saltando, por acionamento luminoso. Este projeto propõe a incorporação de nanoestrelas de ouro que funcionarão como conversores fototérmicos em hidrogéis à base de PNIPAM, o qual possui uma rápida resposta térmica e para temperaturas acima de sua temperatura crítica de solubilidade inferior resulta numa rápida expulsão de água do seu interior. Esta propriedade, juntamente com impressão 3D, pode ser explorada para criar hidrogéis capazes de dobrar e relaxar, que em rápida sucessão, poderá traduzir-se em movimento vertical. Os resultados mostram que as estruturas 3D foram capazes de passar de um estado inicial plano para uma curvatura de 400°, com estímulo térmico de 44°C. Com estimulação luminosa, os hidrogéis incorporados com nanoestrelas de ouro foram capazes de aumentar a sua temperatura 3,6 ° C por minuto. Em meio aquoso, resultou num aumento de 2°C e numa curvatura de 26°, que foi obtida após 2 min de estimulação luminosa, sem alteração mesmo após 10 min. É possível concluir que o calor gerado pelas nanoestrelas de ouro não é suficiente para acionar os *soft robots* num ambiente aquoso devido à dissipação do calor na água.

Palavras chave: Soft robotics, hidrogéis, PNIPAM, nanoestrelas de ouro, impressão 3D, atuação luminosa.

CONTENTS

LIST OF FIGURES

LIST OF TABLES

ACRONYMS

AuNP	Gold nanoparticles
AuNSt	Gold nanostars
GelMA	Gelatin methacryloyl
LCST	Lowest critical solubility temperature
LED	Light-emitting diode
LSPR	Localized surface plasmon resonance
NIR	Near-infrared
PNIPAMMA	Poly(*N*-isopropylacrylamide) methacryloyl
RT	Room temperature
UV	Ultra-violet
Vis	Visible

SYMBOLS

θ	An unknown angle.
r	The radius of a circle.

1

INTRODUCTION

1.1 Motivation

The field of robotics emerged from the need to create autonomous machines that can independently move and perform precise, strong, and repetitive tasks. The elements in these robotic systems are composed of rigid materials, such as stiff plastics, composites, metals, and ceramics. These materials present various advantages, including supporting high loads and large inertial forces. They can maintain constant mechanical and electrical properties under stress conditions and allow precise movement and position through rigid displacements [1]. However, with the advancement of technology and society, new needs emerge. While these robotic systems are precise and reliable, they are not able to adapt to other tasks or operate in an unstructured environment, i.e., a robot built for heavy transportation will not be able to perform precision part assembly, and a robot built to move in a flat terrain will not adapt easily to an unstable environment. Additionally, these robots still struggle with autonomy, as most need to be connected to a power supply. This either makes them static or coupled to a heavy battery. Therefore, robotics must be able to interact with their environment and adjust their response to different conditions. Further, they must be as independent as possible from power supplies and complex processing systems. Thus, a new field of robotics emerged, one that took inspiration from nature. To achieve this, the hard matter was traded for soft matter, and by mimicking simple living organisms, i.e., plants [2] and gastropods [3], the new soft robots were able to move [3], grasp [4] and sense [5]. Thanks to the embedded smartness in the materials, sensing and actuation happen in the same material. Nevertheless, there are still challenges to overcome. Actuation is still very limited and slow due to the materials and the stimuli used, which makes tasks such as locomotion inefficient. Faster stimuli such as light have been used, however requiring specialized tools such as lasers and toxic components such as azobenzene dyes [3].

1.2 Soft robotics

1.2.1 Definition and Applications

Soft robotics is an emerging field that focuses on developing robots manufactured with polymers, elastomers, and other soft materials, as opposed to conventional robots that are constituted of hard materials such as metals, plastics, and ceramics. This allows the creation of machines with flexible actuation and the capacity to adapt themselves to various tasks [6]. Namely in activities that require interacting safely with humans, such as collaborative work [7] and healthcare [8]. The nature of soft robots allows them to be used in biomedical applications since they can be scaled to any desired size and are made of biocompatible materials since most are soft matter. A good example is surgery and endoscopy, enabling the manipulation of the insides of the human

body with minimal incisions, reducing surgery-caused trauma, and lowering the recovery time and scar formation [9]. Due to their flexibility, they are also proficient at navigating hazardous environments with tight spaces, underwater [10] and outer space [11].
Nonetheless, soft robotics still depend on conventional robotic technology, such as electronics, sensors and controllers, and mechanical systems, such as pneumatics [12]. This makes them complex and energy-dependent. Therefore research is working towards tetherless and energy-efficient soft robotics. The system needs to be as simple and independent as possible. Soft robots resort to biomimicry since living organisms are incredibly efficient at simplifying complex tasks. They achieve this through sensory-motor behavior and highly flexible response to dynamic changes. The secret of natural systems lies in the smart characteristics of how their body is designed and how their intelligence is embodied and distributed, allowing them to adapt, grow and survive effectively. Here lies the link with soft robotics: similarly, soft robots benefit from using smart and multi-functional materials (hydrogels [13], elastomers [14], biological materials and more [7]) and a body compliant with the external environment [15].
Many types of responsive materials can imbue soft robots with smartness and flexibility. Dielectric elastomers are electroactive polymers that use electrical stimulation to contract. Their actuation speed is very high, however, for the shape change to happen, a high voltage must be applied to the elastomer, which raises safety concerns [14]. Shape memory polymers are responsive materials capable of being programmed to arbitrary shapes under specific external stimuli, such as heat or light. They are capable of direct motions besides expansion and contraction. Nevertheless, they need to be trained beforehand and suffer from a long transition time due to the cooling process [16]. Liquid crystal elastomers represent a type of thermoplastic elastomer that uses liquid crystal molecules as a physical crosslink. Liquid crystal elastomers were shown to produce actuation strains comparable to mammalian skeletal muscles [17]. However, miniaturization and long-lived deformation of liquid crystal elastomers are still challenging [18].

1.2.2 Hydrogel Soft Robots

Hydrogels are crosslinked polymeric networks that can bind high water content. For this reason, they can drastically change their volume when externally stimulated, usually by changing the hydrogel's affinity with water. Furthermore, unlike the other types of responsive material, hydrogels can be adjusted to respond to various stimuli. These stimuli can be physical such as temperature [19], electric fields [20], and light [21], or chemical, such as pH [22] or biomolecules [23]. Additionally, some hydrogels possess self-healing abilities [24], which allow for multiple actuation cycles without wear. These characteristics make hydrogels very appealing for soft robotics. However, hydrogels with a high water content are susceptible to dehydration in low humidity environments, limiting their robust and long-term use in robotic systems. Nevertheless, using hydrogel-based soft robots in aqueous environments removes this limitation, making them an excellent option.
Hydrogels possess the ability of linear expansion and contraction, thereby introducing anisotropy in the hydrogel makes it possible to bend, fold or twist [25]. The anisotropy causes a swelling mismatch, where certain sections expand or contract more than others, causing internal stress. Anisotropy can be achieved by either single hydrogel structures or multi-material hydrogel structures. Both methods involve introducing different swelling degrees along the structure. For single-material hydrogels, it is possible to achieve this with varying densities of crosslink [19] or due to the introduction of anisotropic particles, such as cellulose nanofibrils, which will expand anisotropically [26]. For multi-material hydrogels, either active and passive layers can be combined to cause internal stress or materials with different triggers, e.g., different transition temperatures.

1.2.3 Light actuation

As mentioned previously, hydrogels can respond to various stimuli. However, stimuli that depend on the diffusion of molecular species, such as pH, ionic concentration, and external field on electroactive conductive hydrogels, exhibit a substantial limitation due to the limited actuation speed. This limitation is not an issue for applications such as grippers and sensors, but a fast actuation is desired for locomotion. Therefore, light is recommended as a stimulus since it permits quick actuation and non-invasive stimulation [13]. Hydrogels can be embedded with fiber functionalized with spiro benzopyran chromophores that change their hydrophilic nature to hydrophobic when stimulated by light [27]. The same can be achieved with azobenzene, which maintains the *trans* conformation under visible light and changes into the *cis* conformation under UV light. The transformation from *trans* to *cis* induces a change in crosslinking density, which can be manipulated to create internal stress [21]. However, azobenzene is toxic and complex to create motion. It would require alternately flashing both light sources to change between forms, making it inconvenient. Alternatively, photo-thermal converters could be embedded in thermo-sensitive hydrogels. There is a great variety of thermo-responsive hydrogels and many photo-thermal converters with tunable sensitivity.

1.2.4 Poly(*N*-isopropylacrylamide)

Poly(*N*-isopropylacrylamide) (PNIPAM) is one of the most used thermos-sensitive hydrogels in soft robotics due to its availability and simplicity. It is characterized by its lowest critical solubility temperature (LCST), which makes it soluble in water for temperatures lower than 32 °C and insoluble in higher temperatures. This behavior can be exploited to produce thermos-sensitive hydrogels. When the temperature is below the LCST, water has an affinity with PNIPAM, therefore the water content increases, expanding the hydrogel. Conversely, if the temperature exceeds the LCST, the hydrogel will contract due to water losing its affinity with PNIPAM, releasing its water content [28]. In this fashion, a soft robot can be tailored to actuate with the LCST of PNIPAM.

PNIPAM soft robots have been achieved by introducing UV shielding inorganic nanoparticles in PNIPAM hydrogels. During the UV cross-polymerization, the nanoparticles protected the PNIPAM from the UV radiation creating a crosslink gradient. When stimulated by heat, a swelling mismatch occurred, allowing the soft robot to bend towards the side with higher content of particles and less crosslinking density [19]. The problem with this technique was the manufacturing time since it was based on a casted mold. Another way to bend with PNIPAM hydrogels was through a multi-material soft robot, where a bilayer was composed of different materials [29]. However, delamination may occur over time due to poor adhesion between layers, thus soft robots should preferably use similar materials to avoid this issue.

1.3 Photo-thermal converters

By resorting to light-sensitive particles, that act as photo-thermal actuators, such as carbon nanotubes, graphene-based particles [30], and gold-based particles, particularly gold nanostars [31] it is possible to convert a light stimulus into a heat stimulus. Gold nanoparticles have been used to create a soft robot capable of swimming while stimulated by a green laser [32]. The problem with this set-up is that the anisotropy comes from the stimulus and not the structure itself, meaning that if the laser points slightly differently, the actuation will also differ. Alternatively, this project aims to create a soft robot capable of swimming triggered by a global light source that illuminates the entire soft robot. However, this global actuation comes with a price. Since a LED light source has less power than a laser, the photo-thermal units in a soft robot need to be more efficient to have the same effect. Another possibility for untethered heating could be magnetic particles since they have

also been used in hyperthermia treatments, achieving very high temperatures. However, magnetic particles need complex machinery to produce heat due to their heating mechanism.

1.3.1 Plasmon effect

Gold nanoparticles have been studied for their numerous properties, namely their optical response [33]. When subjected to an electromagnetic field, the electrons on the nanoparticle's surface will collectively oscillate in resonance with the propagating electric field. This phenomenon is denominated as localized surface plasmon resonance (LSPR) [34]. Another essential feature of plasmonic nanoparticles is the ability to transform light in the visible and near-infrared spectrum into heat. Due to the decay of plasmonic excitations in an oscillating manner, there is the generation of high-energy electron-hole pairs. Since these pairs are not in equilibrium, they tend to release their energy through heat. For that reason, these electrons and holes are frequently referred to as hot carriers [35], [36].

In addition to spheres and spherical shells, gold nanoparticles can be synthesized as rods, triangular prisms, cubes, stars and more [37], [38]. Since size and shape heavily affects the LSPR, the variety of possible morphologies provides a mechanism to manipulate the wavelength at which they resonantly absorb or scatter light [36]. Star-shaped gold nanoparticles have excellent heat generation efficiency due to their plasmon mode combining the plasmon associated with the spherical core and the protruding tips surrounding it. The core is the primary source of hot carriers, boosting the electrical field. The localization of the electric field intensity at the tips causes a significant dephasing of the oscillating surface electrons. This increases the energy transfer to the atomic lattice, resulting in higher heat flux, often called a hot spot [34].

For these reasons, gold nanostars (AuNSt) are an emerging alternative to near-infrared-absorbing nanoparticles, nanoshells, and nanorods because they have a high absorption-to-scattering ratio at their corresponding LSPR and are one of the most effective agents for converting photon energy into heat [34], [36]. Additionally, they are very stable, as other shapes have been known to reshape under intense radiation, e.g., rods, which would shorten their use as converters [39].

1.4 3D Printing of hydrogels

Soft robotics have been using cast molding as a technique to produce soft robots. However, these are either incompatible or not viable with multi-material structures. 3D Printing allows for localized actuation by printing stimuli-sensitive inks in desired patterns. It also introduces anisotropy during printing by choosing different infill types and variable crosslinking cure time. Extrusion-based 3D printing is a technique that allows for multiple materials to be deposited alternately or successively. In this technique, precursor gels (also called inks) are loaded into cartridges and deposited with compressed air layer by layer into a platform (called the printing bed). The precursor gel can be crosslinked after each layer deposition or after the print is completed. Since custom designs can be utilized, this allows the creation of soft robots with localized actuation. However, precursor gels must fulfill some requirements, namely good extrudability and shape fidelity. Extrudability describes the behavior of the precursor gel during extrusion and is related to the minimum pneumatic pressure to extrude the material [40]. It can be altered by modifying the precursor gel's storage and loss modulus, which depends on the polymer's concentration and molecular weight. The viscosity should be high for printing purposes so that the precursor ink does not drip from the nozzle. Due to the polymeric nature of the precursor gels, they naturally exhibit shear-thinning behavior. Where the viscosity decreases as shear stress increases [41], which allows high viscosity inks to be extruded at lower pressures than Newtonian inks. This phenomenon happens because, during the extrusion, the polymers present in ink align with the nozzle. Shape fidelity describes the behavior after extrusion. Once deposited, the filament must regain its original viscosity, or it can

flow and lose the desired shape, creating broader and shorter shapes. Some 3D printers have the option to lower the temperature of the printing bed. This option allows the gelation of ink, increasing the viscosity, which can be used to preserve the shape.

1.4.1 Gelatin methacryloyl

Gelatin methacryloyl (GelMA) consists of gelatin chemically functionalized with methacryloyl groups, forming covalently crosslinked hydrogels through photo-initiated polymerization [42]. Naturally, gelatin physically crosslinks to form a network. Since GelMA is physically crosslinked, raising its temperature above the gel-sol transition temperature (25-30 °C) will break the hydrogen bonding. This break results in a rapid decrease of the elastic modulus, decreasing viscosity and increasing the shear-thinning behavior. Therefore, this hydrogel can be used as a precursor ink since it can be extruded at much lower pressures. However, if the temperature rises above a certain threshold, the ink will lose the required viscosity to maintain its shape after printing. GelMA hydrogels have higher tensile strength than PNIPAM hydrogels, 577.3 kPa [43] and 5 kPa [44], respectively, making the soft robot more resilient.

2

MATERIALS AND METHODS

2.1 Materials

Sodium chloride (NaCl), 4-(2-hydroxyethyl)piperazine-1-ethanesulfonic acid (HEPES), phosphate-buffered saline (PBS), gelatin from porcine skin (Gel strength 300, Type A), methacrylic anhydride (MA) and lithium phenyl-2,4,6-trimethylbenzoylphosphinate (LAP) were purchased from Merck.
Tetrachloroauric(III) acid ($HAuCl_4$), poly(*N*-isopropylacrylamide) amine terminated (PNIPAM), polyvinylpyrrolidone (PVP) Mw = 10000, rhodamine B isothiocyanate (ICT) and *N*-Hydroxysulfosuccinimide sodium salt (NHS) were purchased from Sigma Aldrich.
1-Ethyl-3-(3-dimethylaminopropyl)carbodiimide (EDC) was purchased from TCI.
HEPES-2 buffer consists of 10 mM HEPES and 150 mM NaCl in ultrapure water. AuNSt-HEPES-2 consists of 90% v/v AuNSt dispersion with 10 mM HEPES and 150 mM NaCl in ultrapure water. Ultrapure water (18.2 MΩ cm) was filtered by ELGA Purelab Ultra system (ELGA LabWater, Lane End).

2.2 Methods

2.2.1 Methacrylation of Gelatin

15 g of gelatin were dissolved in 150 mL PBS at 50 °C while stirring until a clear solution was obtained. 9 g of methacrylic anhydride were added dropwise to the clear solution and stirred vigorously for 1 h. 300 mL ultrapure water were added, and the solution was dialyzed against ultrapure water at 40 °C using a cellulose membrane with a cut-off of 3.5 kDa for 5-7 days while protected from light. The product obtained (gelatin methacryloyl, GelMA) was then lyophilized and stored at -20 °C, protected from light. GelMA was labeled with rhodamine B ICT by Stefan Pendlmayr from the Laboratory for Cell Mimicry.

2.2.2 Methacrylation of PNIPAM

23.2 mg methacrylic acid were dissolved in 10 mL HEPES buffer that contained 103.5 mg EDC and 58.6 mg Sulfo-NHS. After 15 min of stirring at RT, 1 g of PNIPAM-NH_2 was added to the solution, which was let to react overnight while stirring at RT. The solution was dialyzed against ultrapure water using a cellulose membrane with a cut-off of 3.5 kDa for 3 days while protected from light.
The PNIPAM methacryloyl (PNIPAMMA) was then lyophilized and stored in a dry environment, protected from light.

2.2.3 Gold nanoparticles

Gold nanoparticles (AuNP) were synthesized via a standard citrate reduction, where sodium citrate was added to a boiling aqueous solution of $HAuCl_4$ and left to react for 15 min under continuous stirring [45] Transmission electron microscopy (TEM) images were obtained for particle characterization by drying a 10 μL droplet,

and their average diameter was measured in ImageJ. In addition, the visible light and near-infrared (Vis-NIR) absorbance was measured in a Perkin Elmar Insight multi-plate reader.

2.2.4 Gold nanostars

The seeds used to grow AuNSt were prepared by coating the AuNP with PVP and left overnight in an orbital shaker. Aqueous solutions of 131 mM $HAuCl_4$ and 0.187 mM AuNP seed dispersion were added simultaneously to 15 or 30 mL of 2.5 or 10 mM PVP solution in DMF under continuous stirring at 25 °C for 15 min [45]. The synthesized particles were washed three times in ethanol and centrifuged at 5500 rpm for 15 min in an Eppendorf centrifuge. Finally, the particles were redispersed in 4 or 6 mL of ultrapure water. TEM images and Vis-NIR absorbance were obtained for particle characterization. The photo-thermal effect of the AuNSt was accessed by illuminating 1 mL of the particle dispersion for 3 minutes and recording the temperature values with a thermocouple USB logger.

2.2.5 Ink Preparation

Passive ink: 7.5 % w/v of GelMA was dissolved in a HEPES-2 or AuNSt-HEPES-2 solution with 0.05 % w/v of LAP, stirring at 60 °C. Once the GelMA was completely dissolved, the solution was transferred to a Cellink cartridge, which was stored at 4 °C overnight.
Active ink: 3-12 % w/v of PNIPAM was dissolved in a HEPES-2 or AuNSt-HEPES-2 solution with 0.1 % w/v of LAP. The solution was kept at 4°C until the polymer was completely dissolved. Then, in a second container, 10 % w/v of GelMA was dissolved in a HEPES-2 or AuNSt-HEPES-2 solution with 0.1 % w/v of LAP, stirring at 60 °C. Supporting information for each ink can be found in Appendix Table 1. Once the GelMA was dissolved entirely, it was cooled to room temperature while stirring and then added to the PNIPAM solution, which was also stirring. After 30 s, the mixture was transferred to a Cellink cartridge, which was kept at 4 °C overnight.

2.2.6 3D-Printing

Three layered 18x6 mm rectangles were printed with rectilinear infill to study the effects of different combinations of active and passive layers on the anisotropy and bending of the structures. Both passive and active ink cartridges were inserted into the temperature-controlled printhead of the 3D printer BioX (CellINK, Sweden), where they were left to heat for 30 min at the desired printing temperature. Printing parameters were varied according to the contents of each ink (see Appendix Table 2). The nozzle size was 25G and the printing bed temperature was set to 8 °C. After extrusion, the hydrogel structures were crosslinked using a UV lamp for 30 sec and stored overnight in 5 mL of HEPES-2.

2.2.7 Heat and light cycles

The ability to shape change was studied by filling a 60 mm Petri dish with 15 mL of HEPES-2 and heating it from room temperature (RT) to 44 °C (heat cycle) or by shining a LED lamp 5 cm away for 3 min (light cycle). The bending was measured with Inkscape as depicted in Appendix Figure 1.

3

RESULTS AND DISCUSSION

3.1 3D Printing

3.1.1 Printability

Shape deformation and bending ability heavily depend on the morphology of the construct, therefore, optimization of the printing resolution is essential. To achieve optimal construct printing, it was necessary to identify adequate parameters, such as ink temperature, extrusion pressure, printing speed, and pre-flow delay. These parameters must be optimized depending on the concentration of GelMA [46], which dictates the ink's rheology, affecting the ink's extrudability and shape fidelity of the obtained construct [26]. The rheology of GelMA can be manipulated through its temperature due to its physical crosslink. Therefore, temperature and pressure are critical parameters that need to be optimized to obtain printed lines (filaments) with a homogenous thickness (Figure 1d). Excessive temperatures resulted in ink with low viscosity, unable to maintain the extruded shape (Figure 1a), while low temperatures resulted in the formation of beads (Figure 1c) since the gel was too solid while being printed. Insufficient pressure resulted in incomplete lines (Figure 1b). Printing speed was vital in promoting good adhesion to the printing bed since excessive speed resulted in deformed structures. Finally, the pre-flow delay was essential to ensure the GelMA started to extrude immediately since there was a delay between the shear stress and extrusion. The optimized values for each printing parameter can be found in Appendix Table 2.

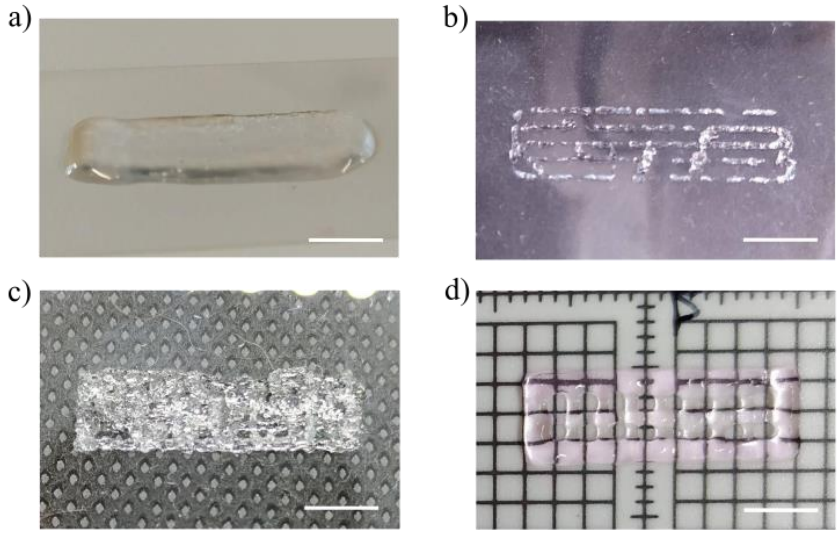

Figure 1 – 3D printing optimization of GelMA precursor gels. Effects of a) Excessive temperature. b) Insufficient pressure. c) Insufficient temperature. d) Adequate parameters.

3.1.2 Anisotropy by fabrication

To print a hydrogel soft robot capable of moving, a swelling mismatch must happen in the structure. Since the goal is to recreate the movements of a fish's tail, the structure needs to bend. This movement can be achieved by introducing anisotropy during the printing process. Otherwise, it would just contract. One way to introduce anisotropy is to manufacture a multi-material hydrogel structure that consists of passive and active layers. Both layers were printed with ink containing GelMA. However, the active layer contained PNIPAM, which presents thermo-responsive properties and will lose affinity with water if the temperature rises above its LCST. This way, the active layer can respond to the stimulus and expulse its water content, which results in a contraction of the hydrogel. Since the passive layer is unresponsive, the swelling mismatch between the layers will cause internal stress resulting in the bending of the structure. Additional anisotropy can be induced by printing rectangular shapes with rectilinear infill (Figure 2a), which will create a structural mismatch causing a more prominent shape change along the longer side of the structure. Therefore to identify each type, layers with active ink in the long direction were denoted as A-type layers and a-type layers if it is in the short direction. For the passive layers, the P-type and p-type layers notation was used. Six PNIPAM-GelMA hydrogel structures were printed with varying positions and numbers of active layers (Figure 2b) to determine which combination of active and passive layers would bend the most. These structures will be denoted as soft actuators since the actuator of a soft robot is a component that generates mechanical motion. This differentiates from the soft robot which is capable of more complex actions, like swimming, pulling and more.

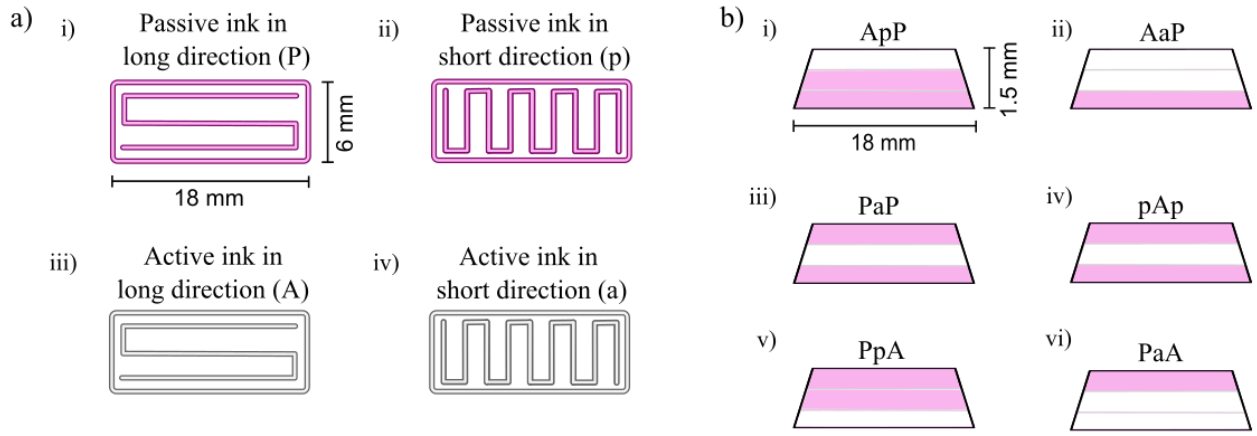

Figure 2 – a) Top view of layer infills for i) P-type layer, ii) p-type layer, iii) A-type layer, iv) a-type layer. b) Side view of printed soft actuators with layer combination i) ApP, ii) AaP, iii) PaP, iv) pAp, v) PpA, vi) PaA.

3.2 Thermal actuation

The shape change induced by temperature was assessed by raising the surrounding temperature of the six soft actuators to 44 °C. Their responses were recorded, and their curvatures were measured with the results observable in Figure 3i. Two sets of structures were examined to understand if the time between printing and stimulation affected the bending capability. One was studied 24 h after they were printed and the second 48 h after. The structure that bent the most was PpA, creating a curvature of 313° (Figure 3e). Comparing it to the structure ApP (Figure 3a), which bent 33°, it is possible to observe that having the active layer as the base increased the curvature by 280°. This difference can originate from the size difference between the active layers. To guarantee good adhesion to the printing bed, the bottom layer was wider in the *xy*-plane but thinner in the *z*-axis than the subsequent ones. This caused the PpA structure to have a longer active layer than the ApP, which can explain the difference in curvature.

However, the same effect was not demonstrated by structures with two active layers, such as AaP and PaA (Figure 3b and f). While also having active layers with different sizes, their curvatures at 44 °C are approximately the same (90°). The difference between these and the PpA and ApP was the presence of an active middle layer, which was not anticipated to bend considerably owing to the infill type. Middle layers are filled along the short side of the rectangle, thus the contraction is more prominent in that direction, which is not favorable to the desired bending. This can be seen when comparing the curvature obtained by PpA and PaA (Figure 3e and f), where the structure with the passive middle layer bent the most. In opposition, comparing ApP and AaP (Figure 3a and b) shows that the structure with a passive middle layer bent the least. The isolated effect of the active middle layer was also studied as the control group. After reaching 44 °C, the construct PaP (Figure 3c) did not considerably bend due to the symmetric structure. Even though the effects of a passive middle layer are not fully understood, it is clear that combining passive middle layers with active bottom layers creates the most efficient bending structure. Therefore the rest of the work will focus on improving the bending of soft actuators with a PpA structure. PNIPAM soft actuators have achieved spiral forms with curvatures of 800°, although in different conditions, such as longer structures and higher concentrations of PNIPAM [19]. Therefore the curvature achieved by the PpA soft actuators may be further optimized.

Comparing the 24 h set with 48 h, it is possible to observe that time does not influence bending since, in most cases, the curvature is approximately the same. However, there are two exceptions, one being PpA, where there is a 135° difference between them (Figure 3e). This variation can result from variable printing quality since the shape and construct thickness heavily affect the soft actuators' performance. The other exception is PaP (Figure 3c), where they reached the same curvature value but in opposite directions. This may be due to small asymmetries induced during the printing process.

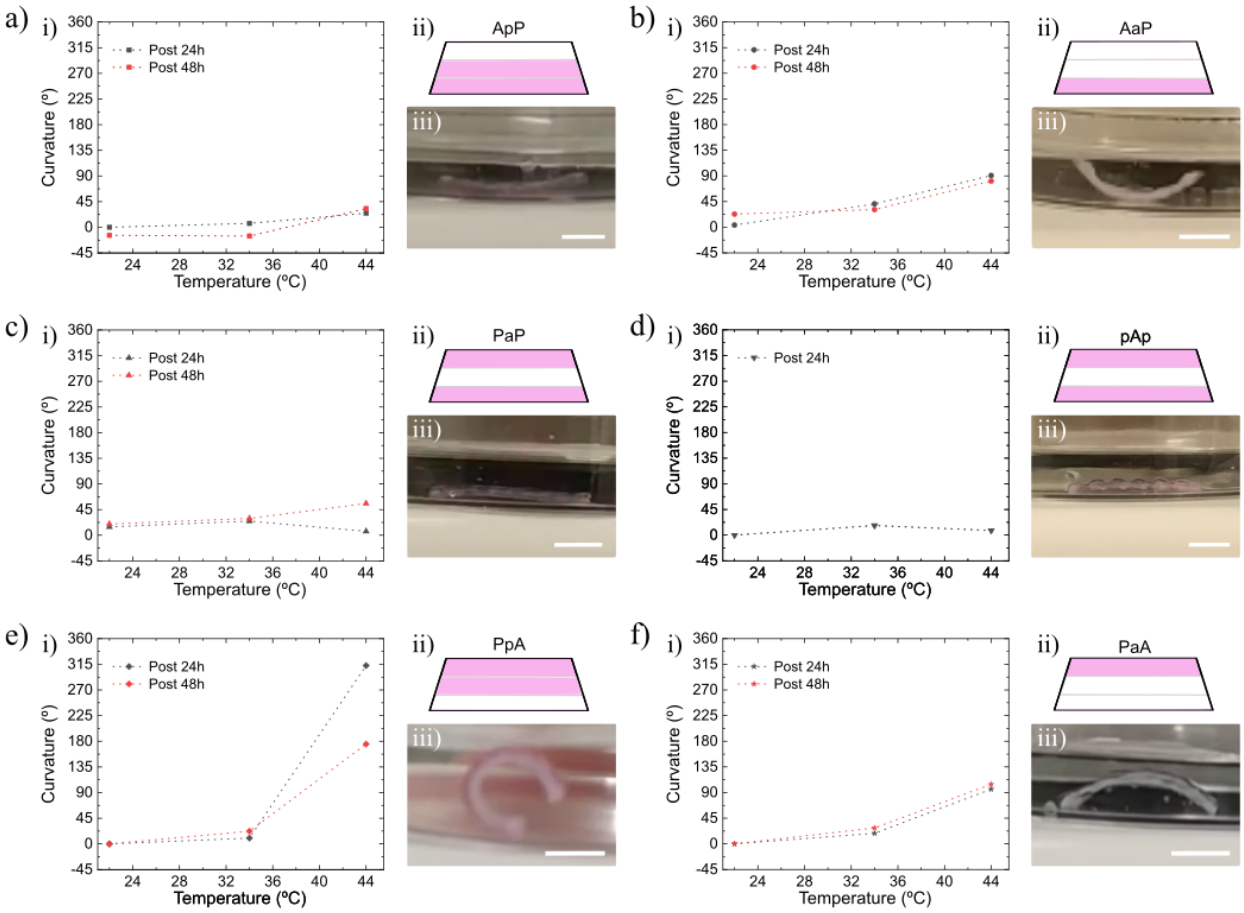

Figure 3 – Thermal shape change of GelMA-PNIPAM soft actuators with a) ApP, b) AaP, c) PaP, d) pAp, e) PpA, f) PaA structure. i) Obtained curvatures at different temperatures 24 h after printing (black lines) and 48 h after printing (red lines). ii) schematic of structure; iii) picture of actuator bending at 44 °C. The scale bar represents 0.5 cm.

3.2.1 PNIPAM Retention

During the initial experiments, although the storage buffer was transparent (Figure 4a), raising the temperature caused the HEPES-2 storage buffer to turn opaque (Figure 4b). However, HEPES does not display an LCST. Therefore, the visible precipitation in Figure 4b could indicate a diffusion of PNIPAM from the soft actuator to the storage buffer. Therefore, a clean buffer was used for each heat cycle to study the actuation instead of heating the sample within the storage buffer. Nevertheless, for the continuation of this study, the problem needed to be addressed since the PNIPAM diffusion could translate into a potential bending loss. Since PNIPAM is responsible for expulsing the water content out of hydrogel, reducing its concentration could translate into less water being expulsed and consequently less bending.

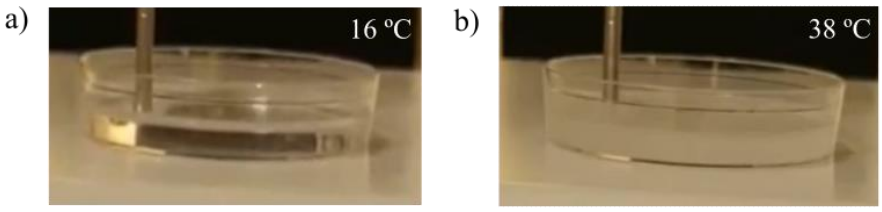

Figure 4 – Visual precipitation of leaked PNIPAM HEPES-2 storage buffer. a) Temperature lower than the LCST. b) Temperature above the LCST.

To determine the mass of PNIPAM that was diffusing from the actuator, a standard curve was used to identify the unknown concentration. The curve was based on the absorbance at 600 nm of PNIPAM solutions at 42 °C, with concentrations from 0.05 to 0.9 mg/mL (Figure 5). The reference value was the PNIPAM mass present in one PpA actuator, estimated to be 0.607 mg (see Appendix A.3), diluted in 5 mL of HEPES-2, the volume of storage buffer. Finally, a sample was collected from the storage buffer of a PpA soft actuator 24 h after printing. The absorbance value obtained was used to extrapolate the mass of the diffused PNIPAM, which was estimated to be 0.38 mg, corresponding to a loss of 62.6 % of the total PNIPAM mass. This is a considerable loss and could translate into potential bending losses.

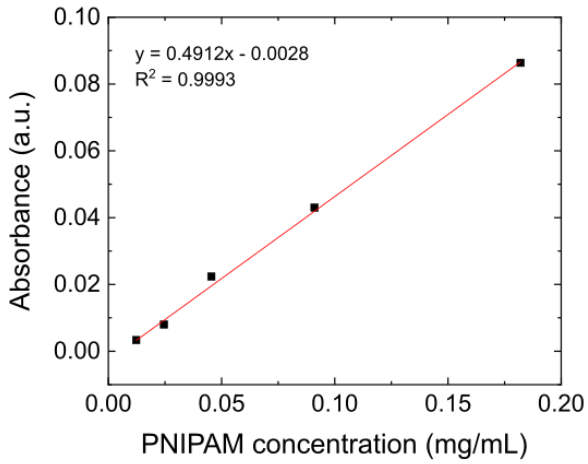

Figure 5 – PNIPAM standard curve recorded at λ = 600 nm for increasing PNIPAM concentrations at 42 °C.

3.2.2 Crosslinkable PNIPAMMA

To reduce the leakage of PNIPAM (Figure 6a) from the soft actuator, the amine end group of the polymer was functionalized with methacrylic anhydride. This functionalization allowed the PNIPAM polymers to crosslink into the GelMA network, preventing its release from the soft actuator. This is the same molecule used to functionalize gelatin into GelMA, allowing the gel to chemically crosslink when cured with UV light. The product of this functionalization was PNIPAMMA (Figure 6b).

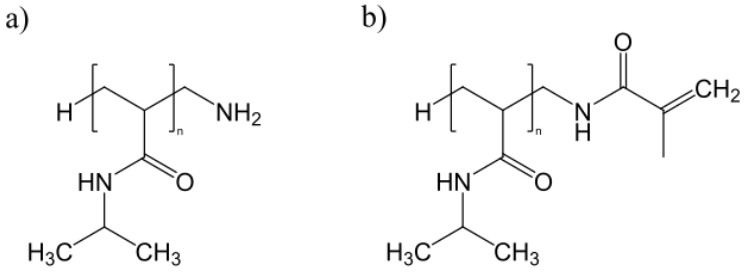

Figure 6 - PNIPAM chemical structures. a) Non-crosslinkable PNIPAM. b) Crosslinkable PNIPAMMA.

To determine the efficiency of the synthesized PNIPAMMA, the leakage of a PpA soft actuator printed with PNIPAMMA ink was measured. The absorbance corresponded to a 32 % loss of the total mass of PNIPAMMA. This leakage could still happen since not all the material was successfully functionalized. Furthermore, not all the PNIPAM molecules were amine terminated as described by the manufacturer, therefore unable to be functionalized. Additionally, some of the PNIPAM molecules could have crosslinked with another PNIPAN molecule, leading to its diffusion into the buffer.

Regarding the effect that PNIPAMMA had on the bending of the PpA soft actuator, after a heat cycle, the maximum curvature measured at 44 °C was approximately 300° (Figure 7b). Since, in the previous experience, the PNIPAM PpA soft actuator had a significant difference between 24 h and 48 h, two new prints were done to discover possible outliers. The repeats achieved similar curvatures of approximately 180°, concluding that this is a more accurate value. With this data, it can be concluded that PNIPAMMA bent 67 % more than non-crosslinkable PNIPAM.

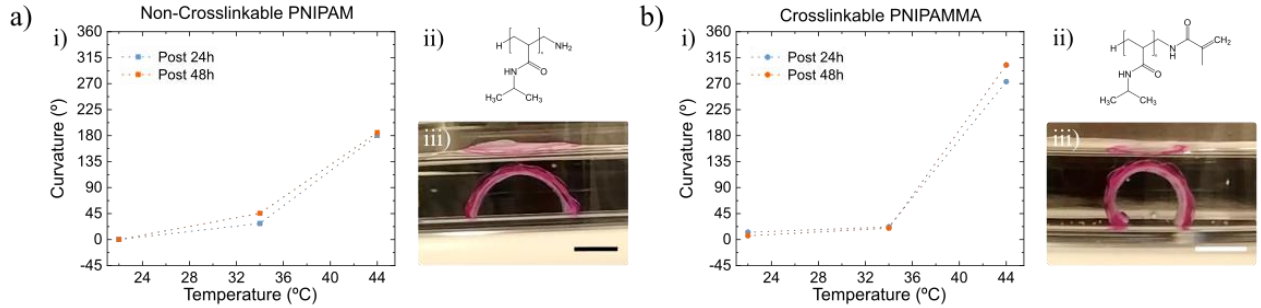

Figure 7 – Thermal actuation of PpA soft actuators with a) Non-crosslinkable PNIPAM. b) Crosslinkable PNIPAM methacryloyl (PNIPAMMA). i) Curvature at different temperatures. ii) Chemical structure. iii) Representative image of the bending at 44 °C. The scale bar represents 0.5 cm.

3.2.3 Swelling ratio

The swelling ratio of the PpA actuators was studied, where three samples were freeze-dried and left in HEPES-2 buffer to swell. Their mass was measured periodically for 24 h, revealing that after 1 h in HEPES-2, the mass of the actuator increased by approximately 1000 %. Furthermore, the maximum swelling was achieved after 6 h, not varying considerably for 24 h. It is possible to conclude that for optimal actuation, the hydrogel soft robots must be kept in HEPES-2 for at least 6 h since their actuation depends on the expulsion of their water content. If sequential actuation is to be considered, it should be expected that the bending achieved by the second actuation will achieve less curvature than the first.

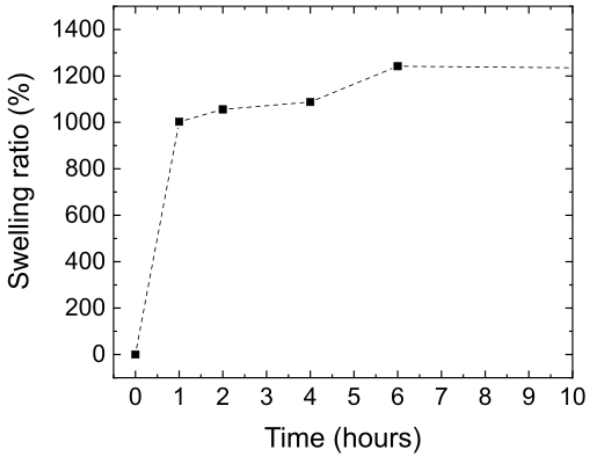

Figure 8 – The swelling ratio of GelMA-PNIPAMMA hydrogels.

3.2.4 Second cycle

An essential characteristic of soft robots is their ability to retain their actuation over several cycles. For this purpose, the PpA soft actuators were submitted to a subsequent heat cycle to ascertain if the actuation still occurs and compare the maximum curvatures. After the first cycle, the soft actuators were cooled down at -10 °C until they became flat, which on average took 3 min. Subsequently, the soft actuators were heated up to 44 °C, and their curvature was measured. In the second cycle, the PpA soft actuators reached a curvature of 225° (Figure 9), which is lower than the one reached in the first cycle. However, the water content must be taken into consideration. While in the first cycle, the soft actuators had 24 h to swell, they only had 3 min for the second cycle. Similar PNIPAM soft actuators managed to maintain the maximum curvature over several cycles, although they needed approximately 12 min to reswell between cycles [19].

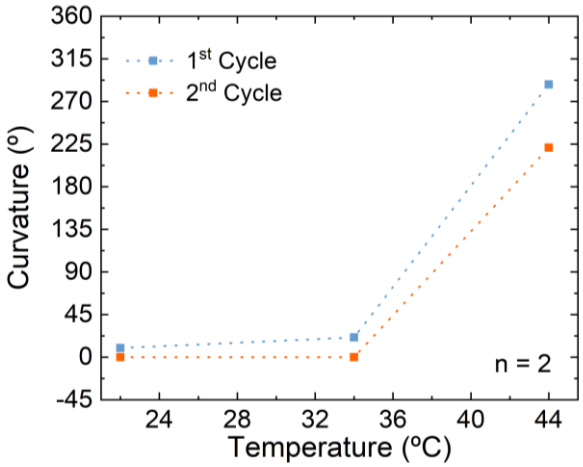

Figure 9 - Thermal actuation of a PpA soft actuator. Curvature achieved in the first cycle of actuation (blue squares) and in the second cycle of actuation (orange squares).

3.2.5 PNIPAMMA Concentration

To investigate the influence of PNIPAMMA concentration, additional PpA soft actuators were printed using inks with initial PNIPAMMA concentrations of 6 % w/v and 12 % w/v (Figure 10). Their bending was compared to the initial 3 % w/v PpA soft actuator (Figure 7b), which will help understand the optimal concentration. Increasing the PNIPAMMA concentration resulted in a decrease in bending. Even though there was a higher concentration of water-expulsing units, in Figure 10a, it is possible to observe that increasing the concentration of PNIPAMMA over 3 % w/v reduces the maximum bending. Since the GelMA concentrations were kept constant, this could have resulted from decreased pore size, resulting in a lower water intake.

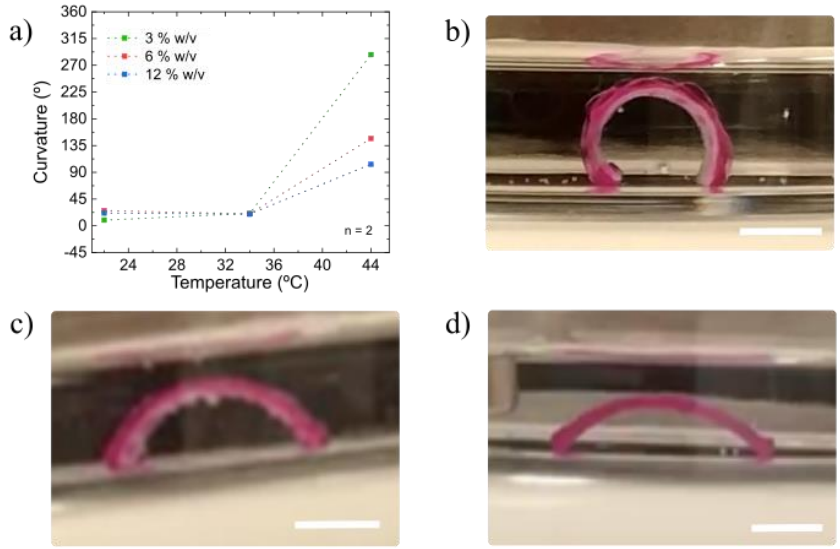

Figure 10 - Effect of PNIPAMMA concentration on the ability to shape change of printed soft actuators. a) Curvature at different temperatures. Representative images of the curvature of PpA soft actuators at 44 °C with PNIPAMMA concentrations of b) 3 % w/v. c) 6 % w/v. d) 12 % w/v. Scale bars represent 0.5 cm.

The leakage of the PpA actuator with different concentrations was also measured (Figure 11). It is possible to observe that the increase in initial concentration led to an increase in leakage. However, if the relative mass is considered, the non-crosslinkable PNIPAM leaks more than the crosslinkable PNIPAMMA.

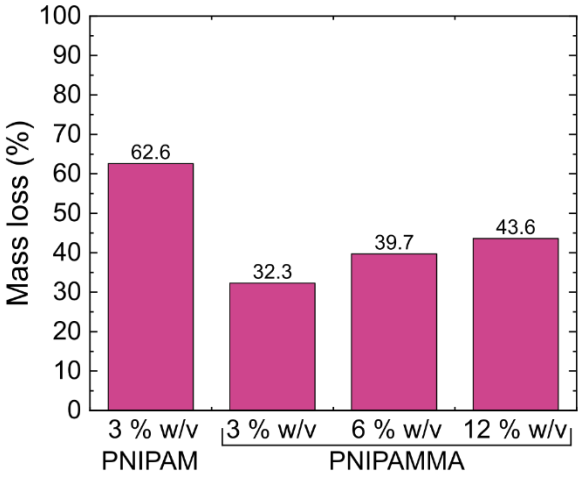

Figure 11 - PNIPAM leakage of actuators with different PNIPAM concentrations.

3.2.6 Altering the LCST of PNIPAMMA

Even though the soft actuators' maximum bending seems to have been optimized, the temperature at which the actuation happens is around 38 °C (Figure 12a), above the LCST of PNIPAM, which is supposed to be 32 °C [28]. This temperature is considerably high, which might not favor the desired photo-thermal actuation. Thus lowering the LCST would be beneficial. The addition of phosphate ions to PNIPAM solutions has been shown to lower the LCST of PNIPAM. This is due to phosphate anions being a kosmotrope in the Hoffmeister series, which organizes anions depending on how hydrated they are. If it is highly hydrated, the anion is considered a kosmotrope; if it is poorly hydrated, it is considered a chaotrope. If kosmotropes are added to a PNIPAM solution, the LCST will be lower since water has a higher affinity with the anions [47]. That explains why the bending occurred at 38 °C since the HEPES-2 buffer possesses dissolved chloride anions that are chaotrope. Therefore to alter the LCST of the PNIPAMMA, the HEPES-2 buffer was substituted to a phosphate buffer and the thermal responsiveness of a PpA soft actuator was studied. In the phosphate buffer, the actuator started

bending at 32 °C instead of 38 °C. Additionally, it increased the maximum curvature achieved by the actuator to approximately 400 ° (Figure 12). This increase in maximum bending can be due to the fact that the water expulsion starts at a lower temperature using a phosphate buffer. Therefore, when the buffer's temperature reaches 44 °C, the volume of water expulsed is higher than the soft actuator's in HEPES-2 at the same temperature. This results in a bigger contraction of the active layer, which translates into more bending.

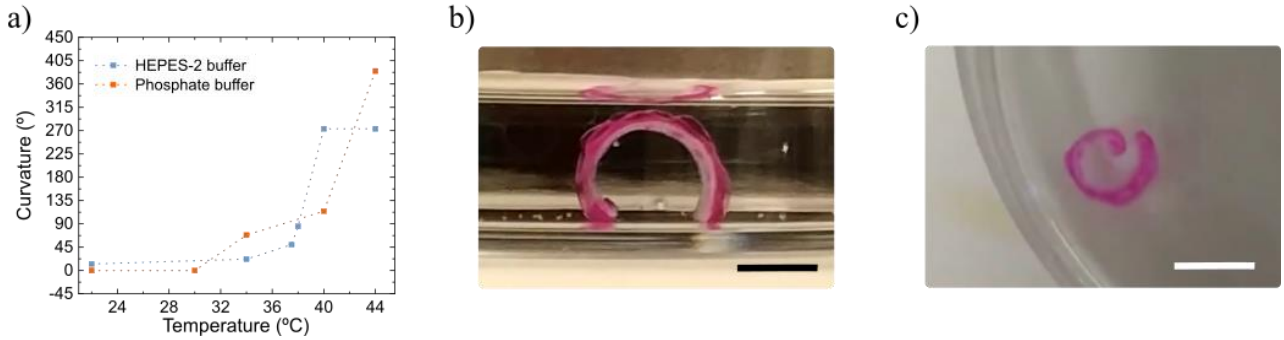

Figure 12 – Effect of the surrounding buffer on the bending of PpA soft actuators. a) Curvatures in HEPES-2 buffer (blue square) and phosphate buffer (orange square). Representative images of curvature at 44 °C of a PpA soft actuator in b) HEPES-2 buffer. c) Phosphate buffer. The scale bar represents 0.5 cm.

3.3 Gold nanostars as photo-thermal converters

3.3.1 Light stimulus

To light-trigger the soft actuators, it is necessary to have a stimulus and a suitable stimuli-responsive unit. A high-intensity white LED light was used for the stimulus due to its accessibility and wide, uniform illumination. Gold nanostars (AuNSt) were chosen as the photo-thermal responsive units since they present a broad absorbance band that can absorb most of the emitted light.

To synthesize suitable AuNSt, it was first necessary to characterize the light source. This way, it would be possible to adjust the particles' synthesis to optimize the photo-thermal conversion. Then, with the help of Jacob Nyemann from the Aarhus University Department of Physics and Astronomy, it was possible to obtain the Vis-NIR emission spectrum of the LED light, which can be seen in Figure 13.

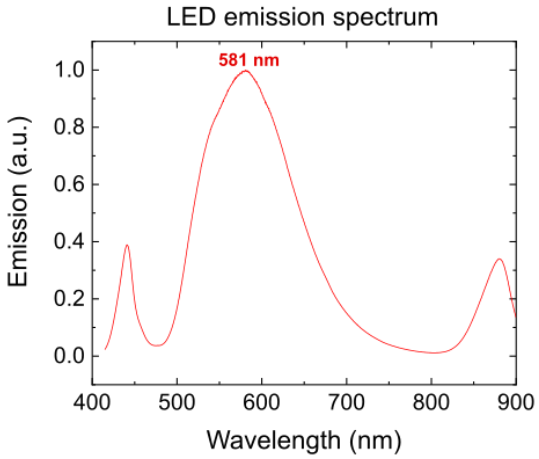

Figure 13 – Vis-NIR emission spectrum of the LED lamp used in photo-thermal actuation, normalized to the peak value, 581 nm.

3.3.2 Gold nanostar morphology

The chosen method to synthesize gold nanostars was a seed-mediated reaction with PVP coating. Via a standard citrate reduction [45], seeds with a diameter of 13 ± 3 nm were obtained (Figure 14b), a standard starting

size to obtain AuNSt capable of absorbing visible light. Fundamentally, the seed size should not be larger than 15 nm since this would shift the absorbance peak into the infrared region [45]. Additionally, the absorbance spectrum was measured (Figure 14c).

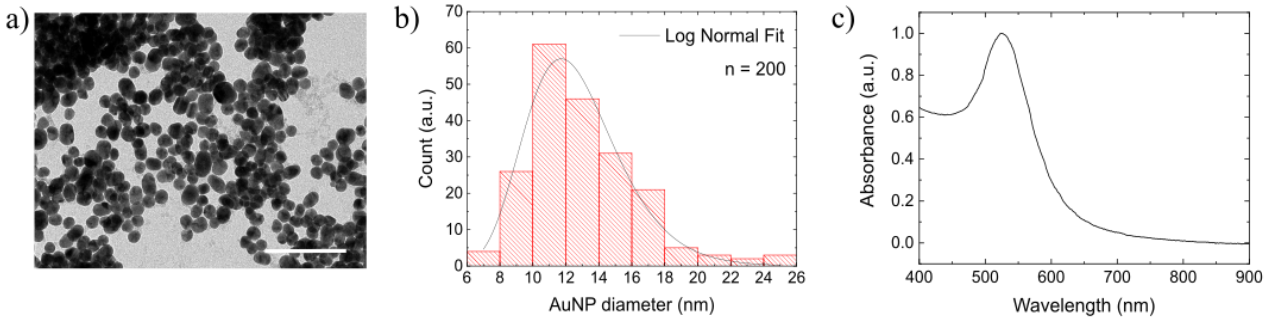

Figure 14 - AuNP characterization. a) Representative TEM image of AuNP, scale bar represents 50 nm. b) AuNP diameter distribution. c) Vis-NIR absorbance spectrum of AuNP dispersion.

To find particles with a high photo-thermal response to the available light source, the synthesis parameters were varied to obtain AuNSt with different morphologies, namely the PVP concentration and $HAuCl_4$-to-Au seed ratio, R. The constituents of each type of particle, named AuNSt 1-5, can be found in Table 1.

Table 1 - Parameters of AuNSt synthesis.

AuNSt dispersion	Seed Coating (µL)	PVP (mM)	R	$HAuCl_4$ (µL)	Au Seed (mL)	Dispersion volume (mL)	AuNSt concentration (mM)
1	117	2.5	12	31.3	0.966	4	4.5×10^{-2}
2	117	10	12	31.3	0.966	4	4.5×10^{-2}
3	117	10	20	31.3	0.575	4	2.7×10^{-2}
4	468	2.5	12	62.6	1.932	6	6.0×10^{-2}
5	468	10	20	110.3	1.932	6	6.0×10^{-2}

In Figure 15i, it is possible to observe the effect each parameter had on the morphology of the stars and how that affected the absorbance spectrum (Figure 15ii). By comparing the TEM images of AuNSt 1 (Figure 15a) and AuNSt 2 (Figure 15b), it is possible to observe that increasing the PVP concentration decreases the size of the star core and increases the size of the spikes. This increase in spike size causes the peak of the absorbance spectrum of the AuNSt to red-shift from 615 to 650 nm. Increasing the R causes the AuNSt 3 to grow a larger core with bigger spikes than previous particles, further red-shifting the absorbance peak from 650 to 688 nm (Figure 15c). It is possible to conclude that the presence of PVP induces the anisotropic growth of the particles, as it enhances the growth in the [011] direction [48]. Since the seeds are polycrystalline, several spikes will grow on their surface. Raising the concentration of PVP in the synthesis further increases the anisotropic growth, increasing the number of spikes and their sizes. However, PVP does not prevent the growth of other crystalline planes, therefore if R increases, thus will the diameter of the particle.

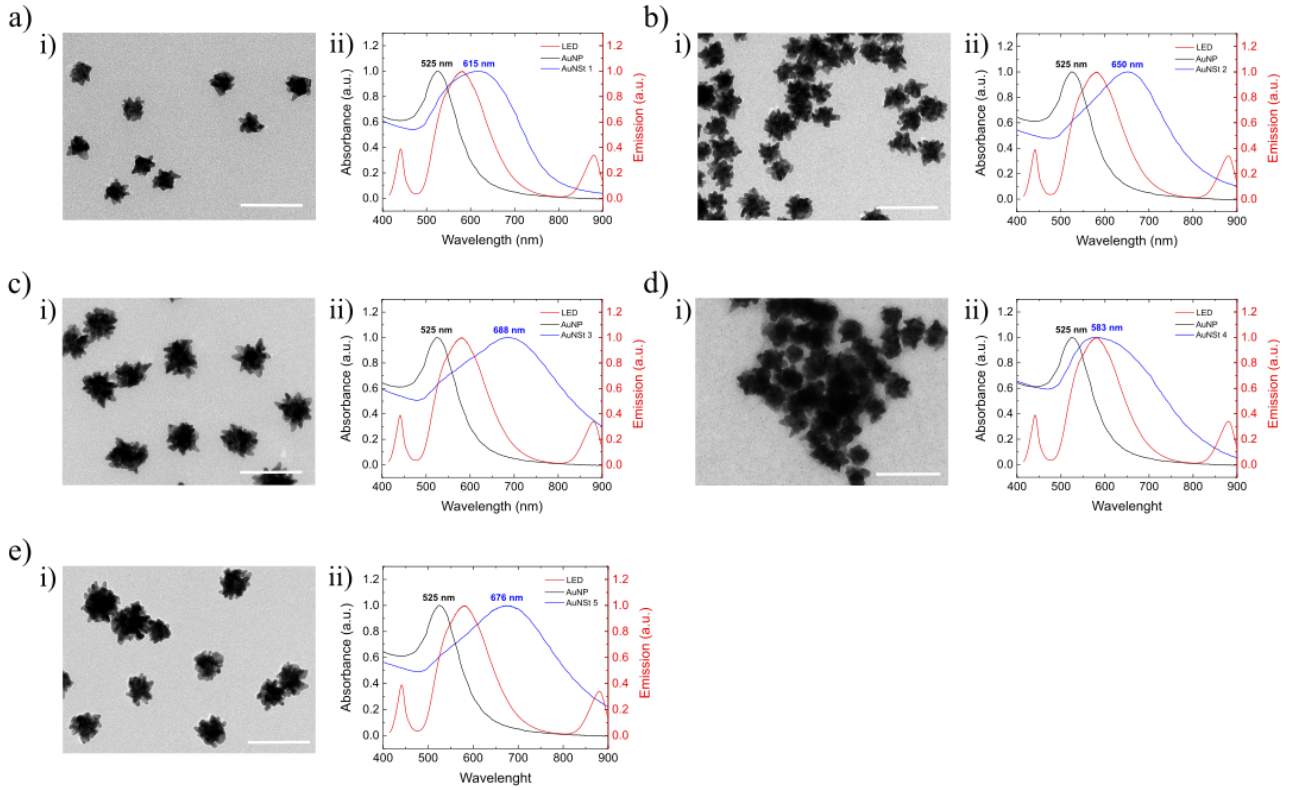

Figure 15 - Characterization of synthesized AuNSt. a) AuNSt 1. b) AuNSt 2. c) AuNSt 3. d) AuNSt 4. e) AuNSt 5. i) Representative TEM image of AuNSt. The scale bar represents 100 nm. ii) Normalized Vis-NIR absorbance spectra of AuNSt (blue), AuNP (black) and emission spectrum of LED light (red).

3.3.3 Photo-thermal effect of gold nanostars

The photo-thermal effect of the AuNSt was accessed through the experimental set-up observed in Figure 16a, with the temperature variations being recorded over 3 min of illumination. The most considerable temperature variation recorded was 11 °C, generated by AuNSt 5, while the smallest variation of 3 °C was generated by AuNSt 1, 2 and 3. It should be noted that AuNSt 3 were synthesized with fewer Au seeds which means that the concentration was lower than AuNSt 1 and 2. Therefore AuNSt 3 could achieve the same temperature with fewer particles, which indicates a more efficient photo-thermal conversion. The increase in diameter and spike size/number considerably influenced the amount of heat generated, even though the peak absorbance did not match the peak emission of the light source. To further study this effect, AuNSt 4 and 5 (Figure 15d and e) were synthesized with the same Au seed concentration but with different R and PVP concentrations (Table 1). After 3 min of illumination, AuNSt 5 increased the temperature of the solution by 11 °C. At the same time, AuNSt 4 increased by 6.5 °C, confirming that both the particle/spike size and the concentration play a significant role in the photo-thermal conversion of AuNSt. This can be explained by the exponential increase of hot carriers present in the core of larger AuNSt and by the increase of spikes. Since the relaxation of accumulated electrons causes the heat in the spikes due to the wavelength excitation, if more electrons are present in the particle, more electron density will be in the spikes. Likewise, if there are more spikes, the heat dissipation will also increase since there are more hot spots [45].

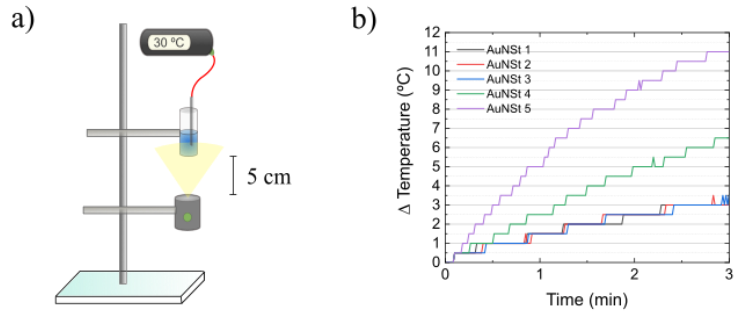

Figure 16 - Photo-thermal effect of AuNSt. a) Schematic of the experimental set-up. b) AuNSt heat profiles after 3 minutes of illumination.

3.4 Photo-thermal actuation

The absorbance was measured in each step of ink preparation to ensure that the particles do not aggregate and thereby cause potential loss of function (Figure 17). The AuNSt 5 dispersed in water (black line in Figure 17) showed a shoulder-shaped absorbance band with a peak absorbance at 676 nm with an intensity of approximately 2.6. Dispersing the AuNSt in HEPES-2 decreased intensity to 2.3 with no change in peak wavelength. Adding PNIPAM does not shift the absorbance peak but decreases the intensity to 2. However, adding GelMA to AuNSt dispersed in HEPES-2 considerably lowers the intensity of the absorbance peak to 1.7 and blue shifts it from 676 to 648 nm. The problem is mitigated when the PNIPAM is added, making the blue shift disappear, although the decrease in intensity remains.

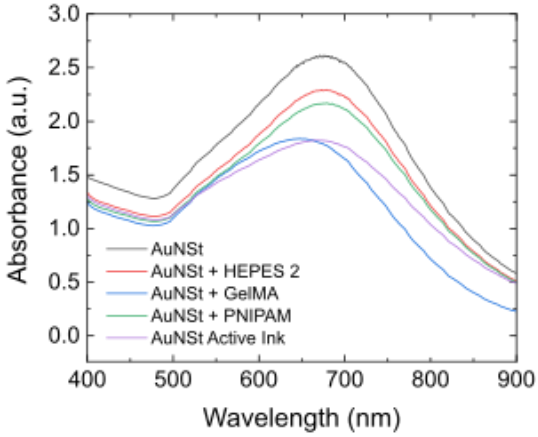

Figure 17 – Vis-NIR absorbance spectra of AuNSt at the different preparation steps of the ink.

3.4.1 Photo-thermal actuators

To test the photo-thermal response of AuNSt in the hydrogel, PpA soft actuators were printed with inks containing AuNSt and were subjected to 5 min of illumination (Figure 18). The experimental set-up can be seen in Appendix Schematic 1. The addition of AuNSt to both passive and active inks altered their rheology. Therefore the printing parameters had to be adjusted (Appendix Table 2), namely the pressure and temperature, which may indicate an increase in viscosity. During the stimulation, only the soft actuator PpA AuNSt 3 (Figure 18a) bent, with the highest curvature obtained after 2 min of illumination (Figure 18aiii). Subsequently, the actuator relaxed, losing curvature (Figure 18av) due to reaching thermal equilibrium with the environment. This can be observed by comparing the temperatures recorded in Figure 18aiv and Figure 18avi, lowering the temperature from 22.3 to 21.9 °C. Since the buffer is not being heated, it dissipates the heat generated by the

AuNSt. In the thermo-camera photos (Figure 18iv), it can be seen that the highest temperature was generated by the soft actuator PpA AuNSt 5 (Figure 18d), which had the particles that caused the highest temperature increase in dispersion. However, no bending was recorded in the PpA AuNSt 5 (Figure 18diii).

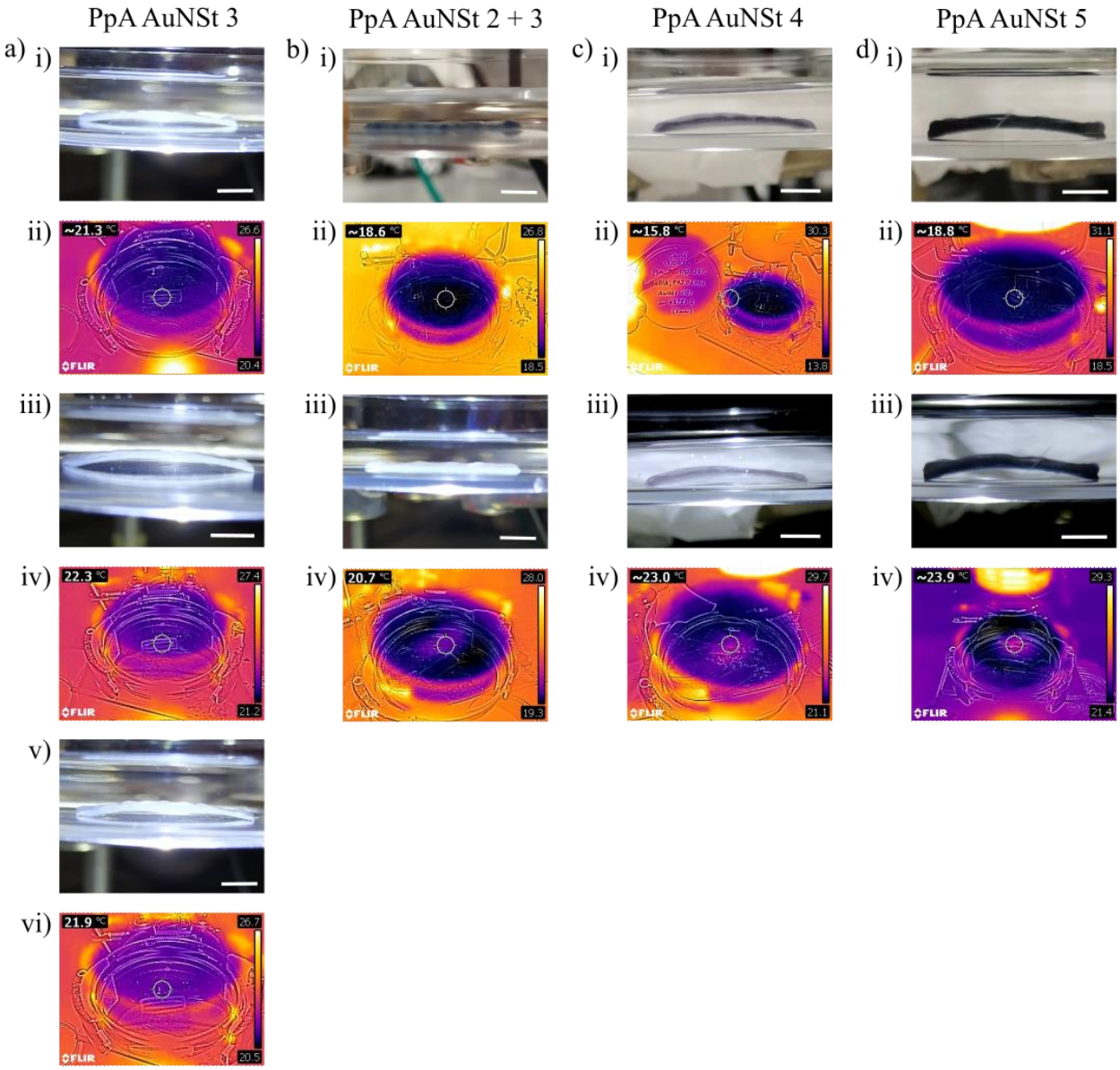

Figure 18 – Bending of photo-thermal actuators. a) PpA AuNSt 3. i) Before illumination. ii) Thermal photo at t = 0 s. iii) Bending after 2 min of illumination. iv) Thermal photo after 2 min of illumination. v) Bending after 5 min of illumination. vi) Thermal photo after 5 min of illumination. b) PpA AuNSt 2 + 3. c) PpA AuNSt 4. d) PpA AuNSt 5. i) Bending before illumination. ii) Thermal photo at t = 0 s. iii) Bending after 5 min of illumination. iv) Thermal photo after 5 min of illumination. The scale bar represents 0.5 cm. Regular photos were taken from a side view, while thermal-photos were taken from a top view.

The temperature reached by the soft actuators was lower than that reached by the AuNSt dispersions, which, the most efficient, raised the temperature by 11 °C. In contrast, the respective actuator only increased the temperature by 4 °C in the buffer. Therefore, to determine the photo-thermal conversion of AuNSt embedded in the gel, the actuator was illuminated outside the buffer to assess the temperature variation (Figure 19). After 3 min of illumination, the soft actuator PpA AuNSt 5 raised its temperature by 11.7 °C, similar to the temperature rise obtained by the AuNSt 5 dispersion (Figure 16). Therefore the AuNSt did not lose their photo-thermal ability. However, they did not generate heat at a faster rate than the dissipation of the water. Therefore, a lower bending was observed. Another possibility is that the AuNSt could have affected the soft actuators' ability to bend.

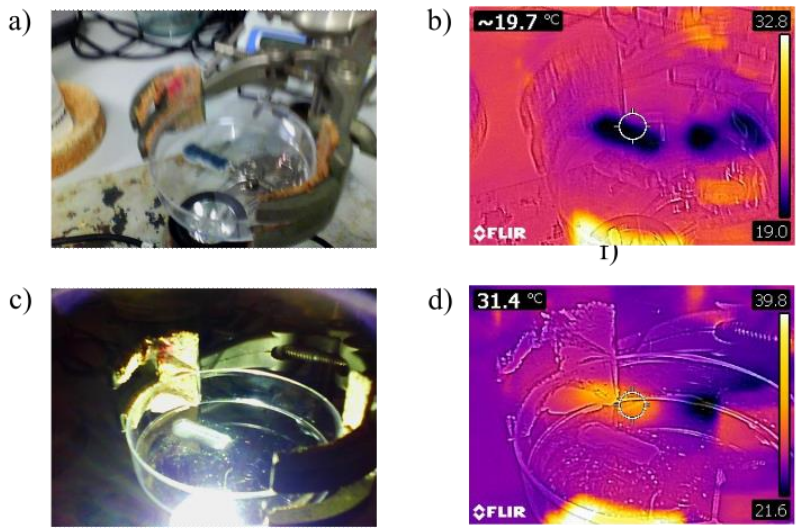

Figure 19 – a) PpA AuNSt 5 soft actuator. b) Thermal photo before illumination. c) Illumination of PpA AuNSt 5 soft actuator. d) Photo-thermal effect of PpA AuNSt 5 soft actuator after 3 min of illumination.

The soft actuators were subjected to a heat cycle to determine if the AuNSt interfered with the soft actuators bending (Figure 20). In Figure 20b, it is possible to observe that the soft actuator PpA AuNSt 3 bent 280°. This value is lower than the curvatures achieved by soft actuators with no AuNSt (Figure 10), which might be explained by the increase in viscosity caused by the addition of AuNSt. This might have increased the force needed to bend the soft actuator.

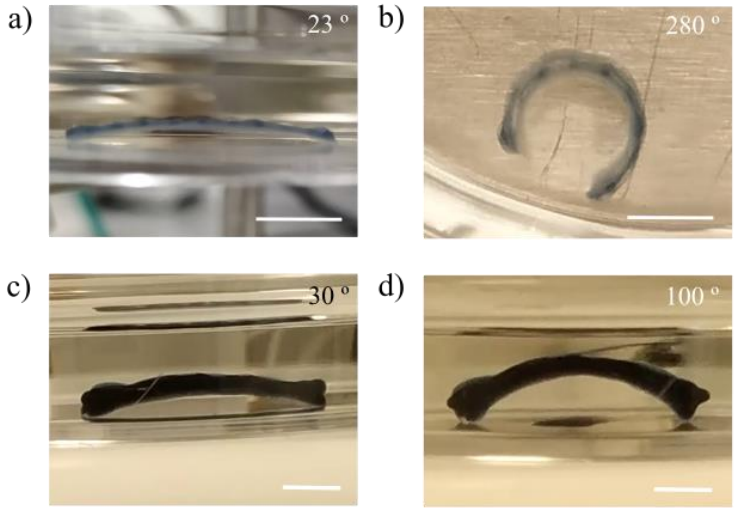

Figure 20 - Thermal actuation of PpA AuNSt soft actuators. a) with AuNSt 3 at RT. b) at 44 °C. c) with AuNSt 5 at RT. d) at 44 °C. The scale bar represents 0.5 cm.

To better understand the internal structure of the actuators, the samples were freeze-dried and observed under scanning electron microscopy (SEM). The images of the cross-section of a PpA AuNSt soft actuator (Figure 21) show that the hydrogel presents a similar pore structure within the hydrogel, indicating a homogenous crosslink. However the structure presents trenches where the crosslink is less dense, showing bigger pores (Figure 21 right). This could indicate that the sample is segmented in different layers, being the sections with lower crosslink density the interface between layers. This could be corroborated by the average printed layer thickness being approximately 500 µm, which matched the distance between two trenches with lower crosslink densities. The close-up SEM picture (Figure 21 right) shows that the hydrogel was not damaged during sample preparation.

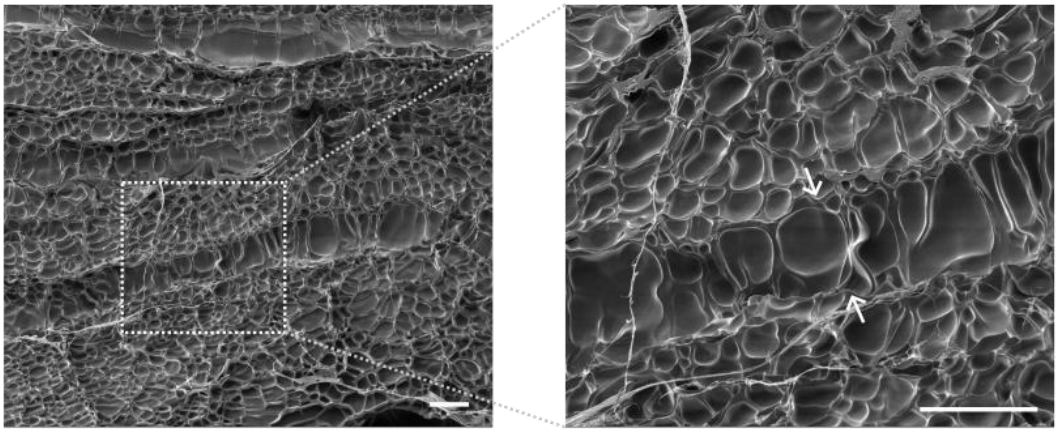

Figure 21 - SEM images of the side view of the PpA soft actuator with AuNSt. The scale bar represents 100 µm.

3.4.2 Photo-thermal soft robots

To manufacture a soft robot capable of swimming, the studied soft actuator was combined with a structure capable of moving. To that effect, a fish-shaped hydrogel was 3D printed (Figure 22) with a PpA actuator in its tail (Figure 22a) and the rest of the body with passive ink. Therefore, the tail will bend when a light source stimulates the soft robot. If the light source is repeatedly turned on and off, presumably, it will cause the flapping of the tail, promoting movement.

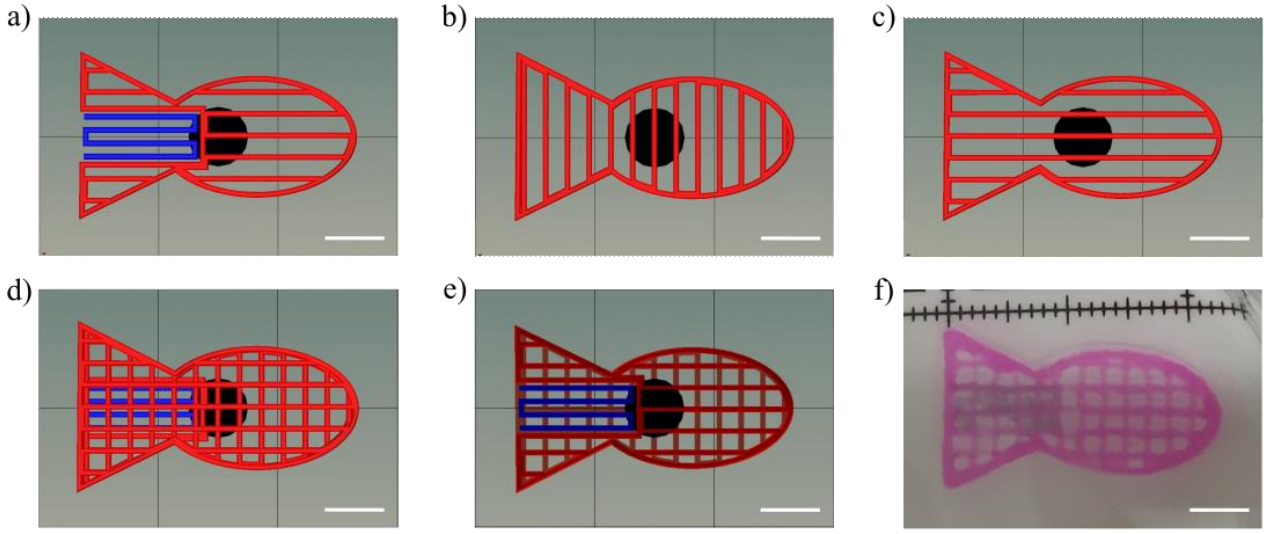

Figure 22 – Preview of 3D printing path for a fish-shaped actuator, with passive ink (red) and active ink (blue). a) Bottom layer. b) Middle layer. c) Top layer. d) Top view of combined layers. e) Bottom view of combined layers. f) 3D printed fish model. The scale bar represents 0.5 cm.

To test its thermal response, the fish soft robot was heated in phosphate buffer with the actuation seen in Figure 23. Bending can be seen as early as 30 °C. However, the most accentuated bending can be seen for temperatures higher than 38 °C. As for the photo-thermal actuation, no change in shape was observed over 5 min of illumination (Figure 23b). A possible explanation is that AuNSt were only present in the active ink, generating insufficient heat to bend the tail. In previous experiments, there was significant heat dissipation to the buffer, and since less ink with AuNSt was used for the soft robot, the effect could have been enhanced. Additionally, the amount of the passive element is higher than the active element, compared to the soft actuators resulting in an imbalance. Thus more bending could be needed since the structure's weight increased. Furthermore, the actuation of the soft robot was slow, which is not beneficial to movement. Therefore new soft robot morphologies and more efficient photo-thermal converters should be studied to make the soft robot more effective.

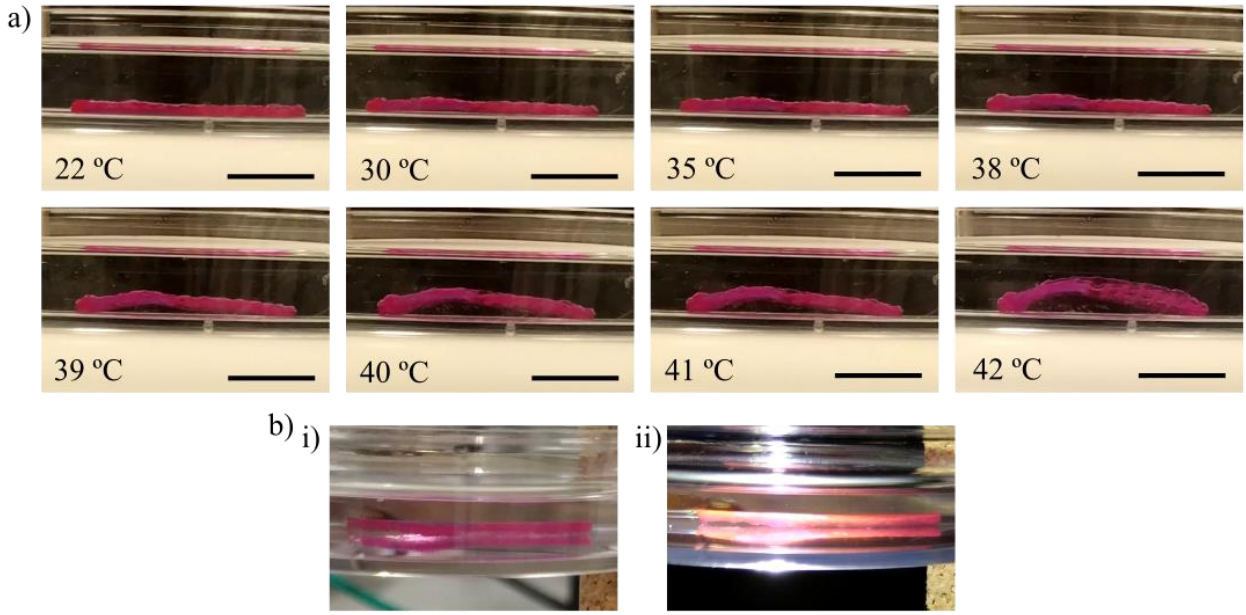

Figure 23 - Soft robot Fish actuation. a) Side view of the thermal actuation of the tail. b) Side view of light actuation of the tail. i) Before illumination. ii) After 5 min of illumination.

4

CONCLUSIONS AND FUTURE PERSPECTIVES

This work's results show that thermally triggered bending soft actuators can be successfully achieved using GelMA-PNIPAM hydrogels. This was possible by optimizing the structural anisotropy from a selection of combinations of active and passive layers. As a result, it was identified that PpA actuators achieved bigger curvatures, as high as 180°. This value was further increased to 312° when the PNIPAM in the active layer was functionalized with methacrylic acid, which allowed it to crosslink into the hydrogel. Furthermore, this functionalization reduced the polymer loss due to leakage from 63 % to 32 %.

However, the actuation was happening at a higher temperature than expected. This effect was due to the HEPES-2 containing NaCl, which has a low affinity with water molecules, increasing the LCST of PNIPAM to 38 °C. To lower the LCST, the buffer was changed to a phosphate buffer with a higher affinity with water molecules than the HEPES-2 buffer. As a result, it lowered the LCST of PNIPAM to 32 °C and increased the maximum curvature to 400°.

AuNSt were successfully synthesized, and by changing the concentration of PVP and the gold salt-to-seed ratio, it was possible to alter their morphology and absorbance spectrum. This led to the optimization of the AuNSt' Vis-NIR photo-thermal conversion, increasing the temperature by 11 °C in 3 min while illuminated, in solution and in gel. However, once the soft actuators were in an aqueous environment, the heat dissipation led to an accentuated decrease of the generated heat to from 11 to 3 °C. Nonetheless, this temperature was sufficient to light trigger the soft actuator PpA AuNSt 3, reaching the maximum curvature after 2 min of illumination. The actuator that achieved this had larger and spikier AuNSt, but with the lowest concentration. This was beneficial to actuation since it made the actuators less viscous. Having achieved a light-triggered soft actuator, the next step consisted of transforming this actuation into movement by incorporating an actuator into the tail of a fish-shaped hydrogel. The fish soft robot successfully bent its tail when stimulated by temperature. However, when the stimulus was changed to light, the fish did not actuate. Possibly the temperature generated was not enough to reach the LCST of PNIPAM and thereby bend the tail since, contrary to the light-triggered actuator, the soft robot fish did not possess AuNSt in all its layers. Therefore future experiments would benefit from studying the effect of AuNSt in both inks of the soft robot. Another possibility to increase the light-triggered actuation would be to change the light source since bigger and spikier AuNSt, which generates more heat, have their maximum absorbance shifted to the infrared region of the spectrum. It is also essential to consider the morphology of the fish since there could be an imbalance of the amount of passive material to active material, making the structure too heavy to bend and needing higher bending strength. Therefore, new structures and shapes should also have priority in future studies.

In conclusion, this study provides additional support for hydrogel soft robotics, introducing an innovative way to increase the durability of PNIPAM-based soft robots by using GelMA as the backbone of the hydrogel. As

for the photo-thermal actuation, it was shown that 3D printing allows the manufacture of soft robots that possess local actuation with a general stimulus instead of the current soft robots that induce a local stimulus via lasers. Additionally, it was shown that AuNSt could be used as photo-thermal converters in soft robotics, a safer alternative than azobenzene and other toxic dyes. However, further effort must be made to improve the conversion, thereby generating sufficient heat to trigger actuation, even when the heat dissipates into the environment. An alternative could rely on AuNSt to light trigger other types of soft robots that do not depend on an aqueous environment to actuate and are temperature responsive, such as liquid crystal elastomer-based soft robots.

The soft robots developed in this work can help improve current soft robotics, which relies on complex techniques or devices. For example, most light-driven soft robots resort to liquid elastomers with azobenzene dyes, which have durability and toxicity challenges. At the same time, other PNIPAM-based soft robots need to use lasers to generate enough heat. Nevertheless, some precision is required to actuate the soft robot correctly. Hopefully, by using simple techniques, soft robotics can become more accessible and be implemented in more applications.

REFERENCES

[1] C. Majidi, "Soft-Matter Engineering for Soft Robotics," *Adv Mater Technol*, vol. 4, no. 2, Feb. 2019, doi: 10.1002/ADMT.201800477.

[2] Y. Cheng *et al.*, "Direct-Ink-Write 3D Printing of Hydrogels into Biomimetic Soft Robots," 2019, doi: 10.1021/acsnano.9b06144.

[3] H. Shahsavan *et al.*, "Bioinspired underwater locomotion of light-driven liquid crystal gels," *Proc Natl Acad Sci U S A*, vol. 117, no. 10, pp. 5125–5133, Mar. 2020, doi: 10.1073/PNAS.1917952117.

[4] C. K. Yoon, "Advances in biomimetic stimuli responsive soft grippers," *Nano Convergence*, vol. 6, no. 1. Korea Nano Technology Research Society, Dec. 01, 2019. doi: 10.1186/s40580-019-0191-4.

[5] H. Mirzanejad and M. Agheli, "Soft force sensor made of magnetic powder blended with silicone rubber," *Sens Actuators A Phys*, vol. 293, pp. 108–118, Jul. 2019, doi: 10.1016/J.SNA.2019.04.021.

[6] C. Majidi, "Soft-Matter Engineering for Soft Robotics," *Adv Mater Technol*, vol. 4, no. 2, pp. 1–13, 2019, doi: 10.1002/admt.201800477.

[7] G. M. Whitesides, "Soft-Robotik," *Angewandte Chemie*, vol. 130, no. 16, pp. 4336–4353, Apr. 2018, doi: 10.1002/ange.201800907.

[8] M. Cianchetti, C. Laschi, A. Menciassi, and P. Dario, "Biomedical applications of soft robotics," *Nat Rev Mater*, 2018, doi: 10.1038/s41578-018-0022-y.

[9] S. Fusco *et al.*, "An Integrated Microrobotic Platform for On-Demand, Targeted Therapeutic Interventions," *Advanced Materials*, vol. 26, no. 6, pp. 952–957, Feb. 2014, doi: 10.1002/ADMA.201304098.

[10] R. K. Katzschmann, J. DelPreto, R. MacCurdy, and D. Rus, "Exploration of underwater life with an acoustically controlled soft robotic fish," *Sci Robot*, vol. 3, no. 16, Mar. 2018, doi: 10.1126/SCIROBOTICS.AAR3449/SUPPL_FILE/AAR3449_SM.PDF.

[11] C. Shan, X. Ng, and G. Z. Lum, "Untethered Soft Robots for Future Planetary Explorations?," *Advanced Intelligent Systems*, p. 2100106, Jul. 2021, doi: 10.1002/AISY.202100106.

[12] M. T. Tolley *et al.*, "A Resilient, Untethered Soft Robot," *https://home.liebertpub.com/soro*, vol. 1, no. 3, pp. 213–223, Sep. 2014, doi: 10.1089/SORO.2014.0008.

[13] Z. J. Wang, C. Y. Li, X. Y. Zhao, Z. L. Wu, and Q. Zheng, "Thermo- and photo-responsive composite hydrogels with programmed deformations," *J Mater Chem B*, vol. 7, no. 10, pp. 1674–1678, 2019, doi: 10.1039/c8tb02896f.

[14] G. Y. Gu, J. Zhu, L. M. Zhu, and X. Zhu, "A survey on dielectric elastomer actuators for soft robots," *Bioinspir Biomim*, vol. 12, no. 1, Feb. 2017, doi: 10.1088/1748-3190/12/1/011003.

[15] B. Mazzolai *et al.*, "Roadmap on soft robotics: multifunctionality, adaptability and growth without borders," *Multifunctional Materials*, vol. 5, no. 3, p. 032001, Aug. 2022, doi: 10.1088/2399-7532/AC4C95.

[16] J. Shintake, V. Cacucciolo, D. Floreano, and H. Shea, "Soft Robotic Grippers," *Advanced Materials*, vol. 30, no. 29, p. 1707035, Jul. 2018, doi: 10.1002/ADMA.201707035.

[17] H. Tian, Z. Wang, Y. Chen, J. Shao, T. Gao, and S. Cai, "Polydopamine-Coated Main-Chain Liquid Crystal Elastomer as Optically Driven Artificial Muscle," *ACS Appl Mater Interfaces*, vol. 10, no. 9, pp. 8307–8316, Mar. 2018, doi: 10.1021/ACSAMI.8B00639/SUPPL_FILE/AM8B00639_SI_007.AVI.

[18] Z. Shen, F. Chen, X. Zhu, K. T. Yong, and G. Gu, "Stimuli-responsive functional materials for soft robotics," *J Mater Chem B*, vol. 8, no. 39, pp. 8972–8991, Oct. 2020, doi: 10.1039/d0tb01585g.

[19] Z. Chen, Y. Chen, C. Chen, X. Zheng, H. Li, and H. Liu, "Dual-gradient PNIPAM-based hydrogel capable of rapid response and tunable actuation," *Chemical Engineering Journal*, vol. 424, pp. 1385–8947, Nov. 2021, doi: 10.1016/J.CEJ.2021.130562.

[20] Y. W. Kang, J. Woo, H. R. Lee, and J. Y. Sun, "A mechanically enhanced electroactive hydrogel for 3D printing using a multileg long chain crosslinker," *Smart Mater Struct*, vol. 28, no. 9, p. 095016, Aug. 2019, doi: 10.1088/1361-665X/AB325D.

[21] Y. L. Zhao and J. Fraser Stoddart, "Azobenzene-based light-responsive hydrogel system," *Langmuir*, vol. 25, no. 15, pp. 8442–8446, Aug. 2009, doi: 10.1021/LA804316U/SUPPL_FILE/LA804316U_SI_001.PDF.

[22] J. Duan, X. Liang, K. Zhu, J. Guo, and L. Zhang, "Bilayer hydrogel actuators with tight interfacial adhesion fully constructed from natural polysaccharides," *Soft Matter*, vol. 13, no. 2, pp. 345–354, 2017, doi: 10.1039/C6SM02089E.

[23] A. Kawamura, T. Kiguchi, T. Nishihata, T. Uragami, and T. Miyata, "Target molecule-responsive hydrogels designed via molecular imprinting using bisphenol A as a template," *Chemical Communications*, vol. 50, no. 76, pp. 11101–11103, Aug. 2014, doi: 10.1039/C4CC01187B.

[24] R. Adam Bilodeau and R. K. Kramer, "Self-healing and damage resilience for soft robotics: A review," *Frontiers Robotics AI*, vol. 4, no. OCT, p. 48, Oct. 2017, doi: 10.3389/FROBT.2017.00048/BIBTEX.

[25] H. Ding, X. Zhang, Y. Liu, and S. Ramakrishna, "Review of mechanisms and deformation behaviors in 4D printing," *International Journal of Advanced Manufacturing Technology*, vol. 105, no. 11, pp. 4633–4649, Dec. 2019, doi: 10.1007/S00170-019-03871-3.

[26] M. Champeau, D. A. Heinze, T. N. Viana, E. R. de Souza, A. C. Chinellato, and S. Titotto, "4D Printing of Hydrogels: A Review," *Adv Funct Mater*, vol. 30, no. 31, pp. 1–22, 2020, doi: 10.1002/adfm.201910606.

[27] O. Kuksenok and A. C. Balazs, "Stimuli-responsive behavior of composites integrating thermo-responsive gels with photo-responsive fibers," *Mater Horiz*, vol. 3, no. 1, pp. 53–62, Dec. 2015, doi: 10.1039/C5MH00212E.

[28] E. Kutnyanszky, "Addressable Macromolecular Architectures: Towards stimuli promoted motion at the nanoscale," Dec. 2012, doi: 10.3990/1.9789036534611.

[29] J. Qian, R. Xiao, L. Wang, F. Liu, and Z. Wu, "Soft Matter PAPER Multi-responsive PNIPAM-PEGDA hydrogel composite," vol. 17, p. 10421, 2021, doi: 10.1039/d1sm01178b.

[30] B. Han, Y.-L. Zhang, Q.-D. Chen, and H.-B. Sun, "Carbon-Based Photothermal Actuators," *Adv Funct Mater*, vol. 28, no. 40, p. 1802235, Oct. 2018, doi: 10.1002/ADFM.201802235.

[31] X. Wang, G. Li, Y. Ding, and S. Sun, "Understanding the photothermal effect of gold nanostars and nanorods for biomedical applications," 2014, doi: 10.1039/c4ra02978j.

[32] Y. Zhao *et al.*, "Soft phototactic swimmer based on self-sustained hydrogel oscillator," *Sci Robot*, vol. 4, no. 33, Aug. 2019, doi: 10.1126/SCIROBOTICS.AAX7112/SUPPL_FILE/AAX7112_SM.PDF.

[33] J. E. Ortiz-Castillo, R. C. Gallo-Villanueva, M. J. Madou, and V. H. Perez-Gonzalez, "Anisotropic gold nanoparticles: A survey of recent synthetic methodologies," *Coord Chem Rev*, vol. 425, p. 213489, Dec. 2020, doi: 10.1016/J.CCR.2020.213489.

[34] A. M. M. Gherman, S. Boca, A. Vulpoi, M. v. Cristea, C. Farcau, and V. Tosa, "Plasmonic photothermal heating of gold nanostars in a real-size container: multiscale modelling and experimental study," *Nanotechnology*, vol. 31, no. 12, p. 125701, Jan. 2020, doi: 10.1088/1361-6528/AB5D83.

[35] T. P. Rossi, P. Erhart, and M. Kuisma, "Hot-Carrier Generation in Plasmonic Nanoparticles: The Importance of Atomic Structure," *ACS Nano*, vol. 14, no. 8, pp. 9963–9971, Aug. 2020, doi: 10.1021/ACSNANO.0C03004/ASSET/IMAGES/MEDIUM/NN0C03004_M026.GIF.

[36] H. Chatterjee, D. S. Rahman, M. Sengupta, and S. K. Ghosh, "Gold Nanostars in Plasmonic Photothermal Therapy: The Role of Tip Heads in the Thermoplasmonic Landscape," *Journal of Physical Chemistry C*, vol. 122, no. 24, pp. 13082–13094, Jun. 2018, doi: 10.1021/ACS.JPCC.8B00388/ASSET/IMAGES/LARGE/JP-2018-00388S_0009.JPEG.

[37] L. Jauffred, A. Samadi, H. Klingberg, P. M. Bendix, and L. B. Oddershede, "Plasmonic Heating of Nanostructures," *Chemical Reviews*, vol. 119, no. 13. American Chemical Society, pp. 8087–8130, Jul. 10, 2019. doi: 10.1021/acs.chemrev.8b00738.

[38] L. M. Liz-Marzán, "Tailoring surface plasmons through the morphology and assembly of metal nanoparticles," *Langmuir*, vol. 22, no. 1, pp. 32–41, Jan. 2006, doi: 10.1021/LA0513353.

[39] H. Yuan, C. G. Khoury, C. M. Wilson, G. A. Grant, A. J. Bennett, and T. Vo-Dinh, "In vivo particle tracking and photothermal ablation using plasmon-resonant gold nanostars," *Nanomedicine*, vol. 8, no. 8, pp. 1355–1363, Nov. 2012, doi: 10.1016/J.NANO.2012.02.005.

[40] T. Gao *et al.*, "Optimization of gelatin-alginate composite bioink printability using rheological parameters: a systematic approach HHS Public Access," 2019, doi: 10.1088/1758-5090/aacdc7.

[41] S. S. Ramirez Caballero *et al.*, "3-D printing of chitosan-calcium phosphate inks: rheology, interactions and characterization," *Journal of Materials Science: Materials in Medicine 2018 30:1*, vol. 30, no. 1, pp. 1–15, Dec. 2018, doi: 10.1007/S10856-018-6201-Y.

[42] D. Loessner *et al.*, "Functionalization, preparation and use of cell-laden gelatin methacryloyl-based hydrogels as modular tissue culture platforms," *Nat Protoc*, vol. 11, no. 4, pp. 727–746, Apr. 2016, doi: 10.1038/NPROT.2016.037.

[43] D. Gan *et al.*, "Mussel-inspired dopamine oligomer intercalated tough and resilient gelatin methacryloyl (GelMA) hydrogels for cartilage regeneration," *J Mater Chem B*, vol. 7, no. 10, pp. 1716–1725, 2019, doi: 10.1039/C8TB01664J.

[44] G. L. Puleo *et al.*, "Mechanical and rheological behavior of pNIPAAM crosslinked macrohydrogel," *React Funct Polym*, vol. 73, no. 9, pp. 1306–1318, Sep. 2013, doi: 10.1016/J.REACTFUNCTPOLYM.2013.07.004.

[45] S. Barbosa *et al.*, "Tuning size and sensing properties in colloidal gold nanostars," *Langmuir*, vol. 26, no. 18, pp. 14943–14950, Sep. 2010, doi: 10.1021/LA102559E.

[46] A. I. van den Bulcke, B. Bogdanov, N. de Rooze, E. H. Schacht, M. Cornelissen, and H. Berghmans, "Structural and rheological properties of methacrylamide modified gelatin hydrogels," *Biomacromolecules*, vol. 1, no. 1, pp. 31–38, 2000, doi: 10.1021/bm990017d.

[47] Y. Zhang, S. Furyk, L. B. Sagle, Y. Cho, D. E. Bergbreiter, and P. S. Cremer, "Effects of hofmeister anions on the LCST of PNIPAM as a function of molecular weight," *Journal of Physical Chemistry C*, vol. 111, no. 25, pp. 8916–8924, Jun. 2007, doi: 10.1021/JP0690603/SUPPL_FILE/JP0690603SI20061231_041707.PDF.

[48] P. Taladriz-Blanco *et al.*, "Impurities in polyvinylpyrrolidone: the key factor in the synthesis of gold nanostars," *Nanoscale Adv*, vol. 4, no. 2, pp. 387–392, Jan. 2022, doi: 10.1039/D1NA00711D.

A

APPENDIX

A.1 Ink composition

Appendix Table 1 - Composition of passive and active inks used in 3D printing.

Ink	Role	GelMA (% w/v)	PNIPAM (% w/v)	PNIPAMMA (% w/v)	AuNSt type
1	Passive	7.5	-	-	-
2	Active	5	3	-	-
3	Active	5	-	3	-
4	Active	5	-	6	-
5	Active	5	-	12	-
6	Passive	7.5	-	-	AuNSt 3
7	Active	5	-	3	AuNSt 3
8	Active	5	-	3	AuNSt 2
9	Passive	7.5	-	-	AuNSt 4
10	Active	5	-	3	AuNSt 4
11	Passive	7.5	-	-	AuNSt 5
12	Active	5	-	3	AuNSt 5

A.2 Printing parameters

Appendix Table 2 - 3D printing parameters for each type of ink.

	Temperature (°C)	Pressure (kPa)	Speed (mm/s)	Pre-flow (ms)	Post-flow (ms)
1	22	11-13	7	150	0
2	22	9-11	7	150	0
3	22	9-11	7	150	0
4	22	20	5	150	0
5	22	5-6	7	150	0
6	22	11	7	150	0
7	22	7-8	7	150	0
8	22	7	7	150	0
9	25	20	7	150	0
10	24	7	7	350	0
11	23	20	7	150	0
12	24	10	2	150	0

A.3 Curvature measurement

The curvature of the structure was measured through Inkscape, using the tool Ruler to measure the angle of an arch. To facilitate the measurement, a circumference was drawn to match the curvature of the side with active ink (Appendix Figure 1).

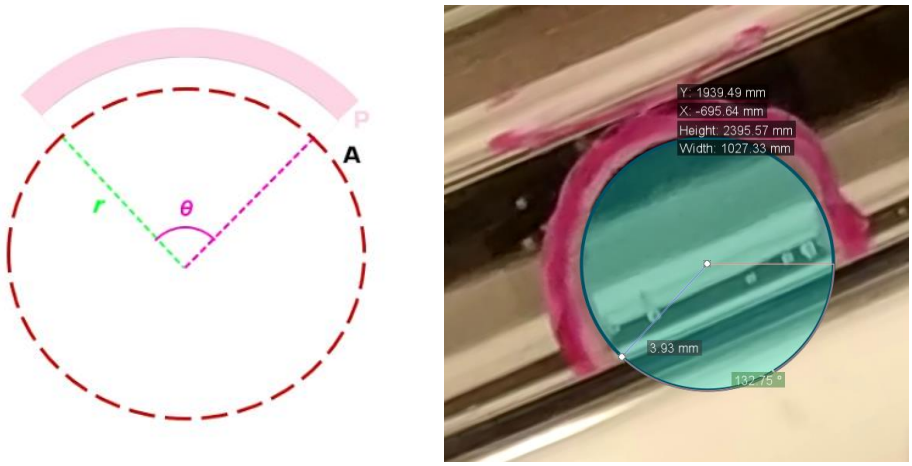

Appendix Figure 1 - Curvature measurement method.

A.4 PNIPAM mass and volume estimation

The PNIPAM mass was estimated by calculating the volume of one layer since it was ascertained that the PpA combination bent the most.

$$V_{Layer} = V_{Perimeter} + V_{Infill}$$

$$V_{Perimeter} = (18 \times 0.5 \times 2 + (6 - 0.5 \times 2) \times 2) \times 0.369 = 10.332\ mm^3$$

$$V_{Infill} = ((18 - 0.5 \times 2) \times 0.5 \times 3 + 1.342 \times 0.5 \times 2) \times 0.369 = 9.905\ mm^3$$

$$V_{Layer} = V_{Perimeter} + V_{Infill} = 10.332 + 9.905 = 20.237\ mm^3$$

By multiplying the volume by the PNIPAM concentration in ink, the estimated value of the mass can be obtained.

$$\frac{w}{v}\% = \frac{\text{PNIPAM Mass}}{\text{Layer Volume}} \times 100 \Leftrightarrow 3 = \frac{\text{PNIPAM Mass}}{20.237} \times 100 \Leftrightarrow$$

$$\Leftrightarrow \text{PNIPAM Mass} = \frac{3}{100} \times 20.237 \Leftrightarrow \text{PNIPAM Mass} = 0.607\ mg$$

A.5 Light Actuation

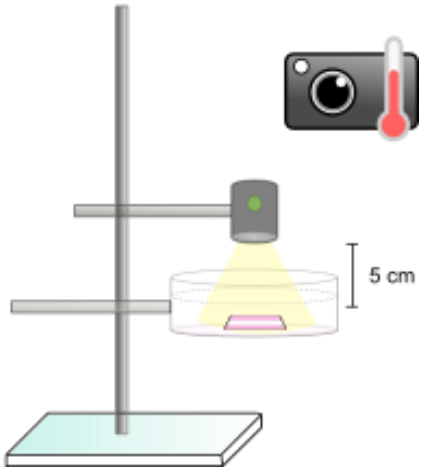

Appendix Schematic 1 - Set-up illustration of for measuring the photo-thermal effect of PpA AuNSt soft actuators.